Electronic Supplementary Material (ESI) for Journal of Materials Chemistry A.

Supporting Information

Fe Nanodots-Decorated MoS_2 Nanosheets on Carbon Cloth: An Efficient and Flexible Electrode for Ambient Ammonia Synthesis

Xinhui Zhao,[a] Xu Zhang,[b] Zhimin Xue,[c] Wenjun Chen,[a] Zhen Zhou,[b] and Tiancheng Mu*[,a]

[a] Department of Chemistry, Renmin University of China, Beijing 100872, China.

[b] School of Materials Science and Engineering, Institute of New Energy Material Chemistry, Key Laboratory of Advanced Energy Materials Chemistry (Ministry of Education), Nankai University, Tianjin 300350, China.

[c] Beijing Key Laboratory of Lignocellulosic Chemistry, College of Materials Science and Technology, Beijing Forestry University, Beijing 100083, China.

* Corresponding Author

Tiancheng Mu: tcmu@ruc.edu.cn

Experimental Section

Materials. Iron(III) chloride hexahydrate ($FeCl_3·6H_2O$, AR), hexaammonium heptamolybdate tetrahydrate ($(NH_4)_6Mo_7O_{24}·4H_2O$, AR), ammonium chloride (NH_4Cl, AR), ethyl alcohol (C_2H_5OH, AR), potassium hydroxide (KOH, AR), polyvinylpyrrolidone K30 (PVP, $(C_6H_9NO)_n$, GR) were purchased from Sinopharm Chemical Reagent Co., Ltd. Salicylic acid ($C_7H_6O_3$, 99.5%), sodium citrate dihydrate ($C_6H_5Na_3O_7·2H_2O$, 99.0%), sodium nitroferricyanide dihydrate ($C_5FeN_6Na_2O·2H_2O$, 99.0%), sodium hypochlorite solution (NaClO, available chlorine 4.0%) were purchased from Macklin Ltd. Thiourea (CH_4N_2S, 99.0%), p-dimethylaminobenzaldehyde ($C_9H_{11}NO$, 99.0%) were bought from J&K Ltd. Sodium borohydride ($NaBH_4$, 98.0%) and hydrazine monohydrate ($N_2H_4·H_2O$, 98.0%) were purchased from Alfa Aesar. Carbon cloth (WOS1009) was purchased from CeTech Co., Ltd. Nafion 212 membrane was obtained from Dupont. Nitrogen (N_2, 99.999%) and argon (Ar, 99.999%) were bought from Beiwen Gas Factory (Beijing, China). All chemicals were analytical grade and used as received without further purification. Milli-Q water of 18.2 MΩ cm^{-1} was used in all experiments.

Synthesis of MoS_2/CC. In a typical synthesis process, hexaammonium heptamolybdate tetrahydrate ($(NH_4)_6Mo_7O_{24}·4H_2O$, 1 mmol, 1.235 g) and thiourea ($SC(NH_2)_2$, 30 mmol, 2.284 g) were dissolved in deionized water (35 mL). After stirring for 30 min, the homogeneous solution was transferred to a 50 mL Teflon-lined stainless steel autoclave. Afterwards, a piece of carbon cloth (2 × 3 cm^2) was placed standing against the wall of the autoclave, sealed tightly, and heated at 220 °C for 18 h. After cooling to room temperature naturally, the carbon cloth was taken out by a tweezer, mildly sonicated in water for 1 min, rinsed with water and ethanol for several times and then dried in an oven at 60 °C overnight. The mass loading of MoS_2 of the MoS_2/CC samples was calculated by the mass difference before and after hydrothermal reaction as approximately 2.0 mg cm^{-2}. And the mass loading of MoS_2 could be controlled by

adjusting the concentration of the precursor solution. Different mass loadings of MoS_2 were prepared with various concentrations of Mo and S precursors, while keeping the molar ratio of $(NH_4)_6Mo_7O_{24}\cdot 4H_2O$ and $SC(NH_2)_2$ as 1:30. According to the previous studies,[1-3] the following chemical reactions were suggested to be involved during the whole conversion process:

$$CS(NH_2)_2 + 2H_2O \rightarrow 2NH_3 + CO_2 + H_2S \quad (1)$$

$$(NH_4)_6Mo_7O_{24} \rightarrow 6NH_3 + 7MoO_3 + 3H_2O \quad (2)$$

$$MoO_3 + 3H_2S + H_2O \rightarrow MoO_2 + SO_4^{2-} + 2H^+ \quad (3)$$

$$MoO_2 + 2H_2S \rightarrow MoS_2 + 2H_2O \quad (4)$$

Synthesis of Fe-MoS_2/CC. To prepare the Fe-MoS_2/CC electrode, Fe nanodots was decorated on the MoS_2 nanosheets surface by using chemical reduction method in the solution of 5 mM $FeCl_3\cdot 6H_2O$ + 1 wt % polyvinylpyrrolidone (PVP) + 0.1 g $NaBH_4$ (50 mL) for 20 min at ambient temperature. The samples were dried in nitrogen flow at 120 °C to remove excess moisture. Fe-MoS_2/CC with different mass ratios of Fe/MoS_2 can be achieved by controlling the concentration of $FeCl_3\cdot 6H_2O$ aqueous solution. The Fe nanodots are formed according to the following chemical reactions:[4]

$$Fe(H_2O)_6^{3+} + 3BH_4^- + 3H_2O \rightarrow Fe + 3B(OH)_3 + 10.5H_2 \quad (5)$$

Characterizations. The XRD patterns of the samples were recorded using an X-ray diffractometer (Rigaku D/Max-2500) using Cu Kα as X-ray radiation (λ = 1.5418 Å) under 40 kV and 30 mA. Data were collected in Bragg-Brettano mode using 0.02° divergence with a scan rate of 2° min^{-1}. The SEM images, EDS spectra and elemental mapping images of the samples were acquired using a Hitachi SU 8010 field emission scanning electron microscope coupled with energy dispersive X-ray spectroscopy operated at 15.0 kV. The samples were prepared by dropping catalyst powder dispersed in isopropanol onto 300 nm silicon dioxide-coated silicon wafer (Zhejiang Lijing Technology Corp., China) using micropipettes and were dried

under ambient conditions. The TEM patterns were carried out using a JEM-2100F transmission electron microscope at 200.0 kV. The samples were prepared by dropping catalyst powder dispersed in isopropanol onto carbon-coated copper TEM grids (Beijing Zhongxing Braim Technology Corp., China) using micropipettes and were dried under ambient conditions. The Raman spectra were conducted using a FT Bruker RFS 106/S spectrometer equipped with a 532 nm laser. X-ray photoelectron spectroscopy (XPS) was performed on the Thermo Scientific ESCALab 250Xi using 200 W monochromatic Al Kα radiation. The 500 μm X-ray spot was used for SAXPS analysis. The base pressure in the analysis chamber was about 3×10^{-9} mbar. Typically, the hydrocarbon C1s line at 284.8 eV from adventitious carbon is used for energy referencing in XPS experiments. UV-vis experiments were performed on a UV-3600 Plus UV-Vis-NIR Spectroscopy (Shimadzu Corp., Japan). The hydrogen production amount at different potentials was measured by a calibrated gas chromatograph (Agilent 7890A).

DFT calculations. The density-functional theory (DFT) calculations in this work were performed using the Vienna Ab-initio Simulation Package (VASP). The projector augmented plane wave (PAW) method was used to describe the interactions between ion cores and valence electrons.[5] The electron exchange-correlation interaction was treated using the generalized gradient approximation (GGA) with the Perdew-Burke-Ernzerhof (PBE) functional.[6] The plane waves with a cutoff energy of 400 eV were used, and the 3×3×1 Monkhorst-Pack grid k-points were employed to sample the Brillouin zone integration. The structures were optimized until the energy and the force were converged to 1.0×10^{-5} eV/atom and 0.02 eV/Å, respectively. All calculations are fully spin polarized.

$$\Delta G = E_{DFT} + E_{ZPE} - T\Delta S \qquad (6)$$

where E_{DFT} is the DFT calculated energy, E_{ZPE} and TΔS are calculated by DFT vibration frequency analysis, and presented in Table S3-S5, whereas the thermodynamic corrections for gas molecules were from standard tables.[7]

Over these optimized structures, vibrational frequencies were calculated in order to obtain zero-point energies (ZPE), thermal corrections and entropy contributions. All Gibbs free energy values for the N_2 reduction mechanism were referenced to the Computational Hydrogen Electrode (CHE) model using the Proton-Coupled Electron Transfer (PCET) approach.

Throughout this work, we used a large super cell (18.978 × 18.370 × 25.044 $Å^3$), which contains six, four elementary MoS_2 units in the x and z directions, respectively, and one layer along the y-axis. A vacuum layer of 15 Å is located above the MoS_2 slab in the z direction to avoid interactions between slabs. Since the molecules are adsorbed only on one side of the slab, dipolar corrections have been added in the z direction. As shown in Figure S45, the calculated energy barrier in the PDS on S edge of MoS_2 is much lower than that value on Mo edge, so we choose free-energy on S edge of MoS_2 to compared with Fe-MoS_2.

Electrochemical measurements. Before NRR tests, the Nafion 212 membrane was pretreated by heating it in H_2O_2 (5%) aqueous solution at 80 °C for 1 h and ultrapure water at 80 °C for another 1 h, respectively. The electrochemical experiments were conducted on CHI 660E electrochemical workstation by using a three-electrode configuration with Fe-MoS_2/CC working electrode, graphite rod counter electrode and Ag/AgCl (saturated KCl electrolyte) reference electrode. All potentials were converted to reversible hydrogen electrode (RHE). The as-obtained Fe-MoS_2/CC sample was cut into 1.0 x 1.0 cm^2 as working electrode with Fe-MoS_2 mass loading of ~2.15 mg cm^{-2} unless otherwise stated.

For electrochemical NRR, potentiostatic tests were carried out in N_2 saturated diluted potassium hydroxide electrolyte (0.1 M, pH=12.9, 30 mL), which was bubbled with N_2 for 30

min before the measurement. A two-compartment cell with three-electrode configuration was separated by Nafion 212 membrane. Pure N_2 (99.999%) was continuously fed into the cathodic compartment with a properly positioned sparger so that the whole cathode was hit by the gas bubbles during the experiments. The N_2 flow rate is 10 mL min^{-1} because there are no apparent changes in the NH_3 yield rate and FE at different N_2 flow rates (Figure S46). No in-line acid trap was used to capture NH_3 that might escape from the electrolyte in our study, as no apparent NH_3 was detected in the acid trap under our experimental conditions. The potentiostatic NRR tests are conducted at desired conditions for 2h. Unless otherwise stated, all experiments were performed at ambient temperature (25 ± 2 °C) and electrode potentials were converted to the RHE scale using E(RHE) = E(Ag/AgCl) + 0.197 V + 0.059 * pH. The error bars correspond to the standard deviations of measurements over three separately prepared samples under the same conditions.

Electrochemical impedance spectroscopy (EIS). The spectra were recorded using potentiostatic mode at open circuit potential. The data obtained were fitted using the Zview software (Version 3.1, Scribner Associates, USA). The electrical equivalent circuit used for simulating the experimental impedance data has been given in Figure S47.

Determination of ammonia. Concentration of produced ammonia was spectrophotometrically determined using the indophenol blue method with modification. First, 2 mL aliquot of the electrolyte solution was pipetted from the cathode cell, and then mixed with 2 mL of a 1.0 M NaOH solution containing salicylic acid (5 wt%) and sodium citrate (5 wt%). Afterwards, 1 mL of 0.05 M NaClO and 0.2 mL of an aqueous solution of sodium nitroferricyanide dihydrate (1 wt%) were added to the above solution subsequently. After 2 h at room temperature, the absorption spectra of the resulting solution were measured using an ultraviolet-visible (UV-vis) spectrophotometer. The formation of indophenol blue was

determined using the absorbance at a wavelength of 655 nm. The concentration–absorbance calibration curves were built using standard NH_4Cl solution with NH_3 concentrations of 0.0, 0.5, 1.0, 1.5, 2.0, 2.5 and 3.0 μg mL^{-1} in 0.1 M KOH. The fitting curve ($y = 0.418x + 0.042$, $R^2 = 0.999$) shows good linear relation of absorbance value with NH_3 concentration by three separately independent calibrations. The measurements with the background solutions (no NH_3) were performed for all experiments, and the background peak was subtracted from the measured peaks of NRR experiments to calculate the NH_3 concentrations and the Faradaic efficiencies. The produced NH_3 was also measured by ion chromatography (ICS-1000, Thermo Dionex). The eluent was methanesulfonic acid (20 mmol/L) with a flow rate of 1.0 mL/min.

Determination of hydrazine. The hydrazine present in the electrolyte was estimated by the method of Watt and Chrisp. A mixture of p-dimethylaminobenzaldehyde (5.99 g), HCl (concentrated, 30 mL) and ethanol (300 mL) was used as a color reagent to quantify the N_2H_4 concentration. Typically, 5 mL aliquot of the sample solution was taken out from the cathode cell, and then mixed with 5 mL color reagent. After stirring 15 min at room temperature, the absorbance spectra of the resulting solution were measured at 455 nm using an ultraviolet-visible (UV-vis) spectrophotometer. The concentration–absorbance calibration curves were established with known N_2H_4 concentrations of 0.0, 0.5, 1.0, 1.5, 2.0 and 2.5 μg mL^{-1} in 0.1 M KOH. The fitting curve ($y = 0.616x + 0.018$, $R^2 = 0.999$) shows good linear relation of absorbance value with N_2H_4 concentration by three separately independent calibrations.

^{15}N isotope labeled experiment. The ^{15}N Isotope labeled experiment was carried out using $^{15}N_2$ as the feeding gas in 0.1 M KOH electrolyte. The electrolyte was first bubbled with Ar for 30 min to remove $^{14}N_2$ and then purged with $^{15}N_2$. After electrolysis at −0.1 V vs. RHE for 2 h, 10 mL of the obtained NH_4^+-contained electrolyte solution was taken out and acidized to pH ~2 by adding 0.1 M HCl, and then concentrated to 1 mL by heating at 60 °C in an oven.

Afterwards, 0.1 mL of the resulting solution was mixed with 0.9 mL d^6-DMSO for ^1H nuclear magnetic resonance measurement (^1H NMR, Bruker 400 MHz).

Faradaic efficiency. The Faradaic efficiency (FE) was calculated from the total charge Q passed through the cell and the total amount of NH_3 produced. The total amount of NH_3 produced was measured using colorimetric methods. Assuming three electrons were needed to produce one NH_3 molecule, the Faradaic efficiency can be calculated as follows:

$$FE = \frac{3F * c(NH_3) * V}{17 * Q}$$

where F is the Faraday constant (96485 s A mol^{-1}), $c(NH_3)$ is the measured NH_3 concentration, V is the volume of electrolyte.

The rate of NH_3 formation was calculated using the following equation:

$$v(NH_3) = \frac{c(NH_3) * V}{S * t}$$

Where t is the reduction reaction time and S is the electrode geometric area.

FE for H_2 can be calculated as follows:

$$FE = \frac{2F * n}{Q}$$

where F is the Faraday constant; n is the actually produced H_2 (mol), and Q is the quantity of applied electricity.

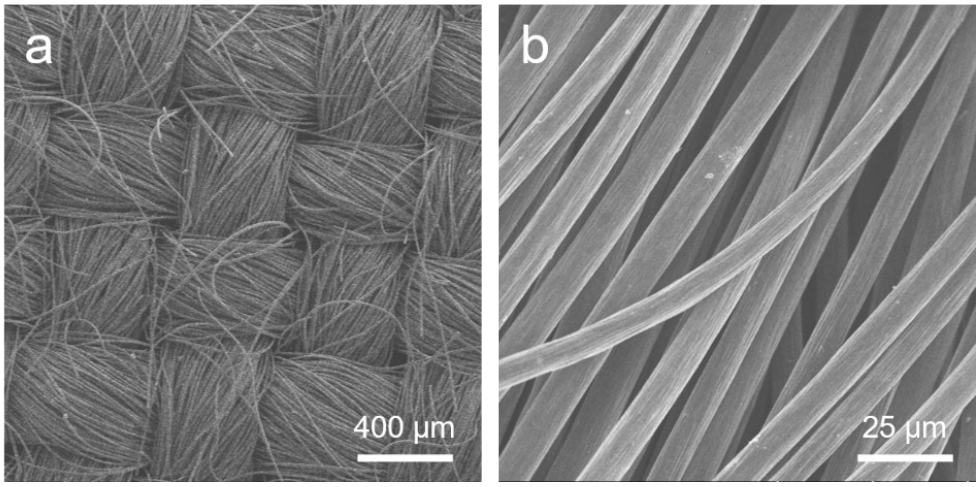

Figure S1. SEM images of bare carbon cloth (CC) fibers.

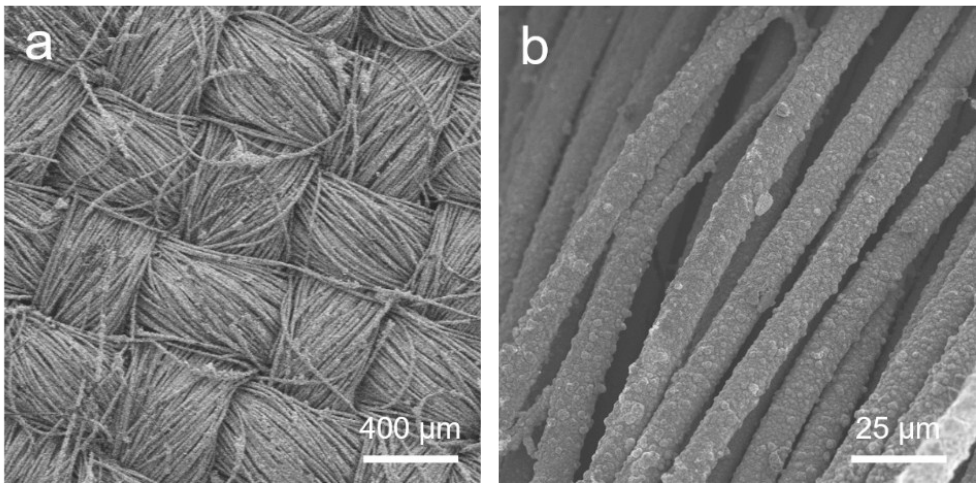

Figure S2. SEM images of Fe-MoS_2/CC.

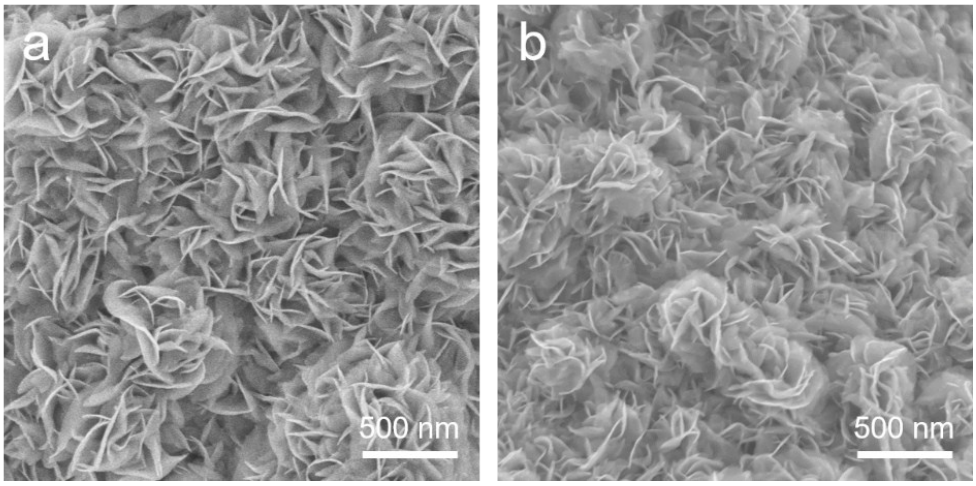

Figure S3. SEM images of MoS_2 nanosheets a) before and b) after Fe nanodots decoration.

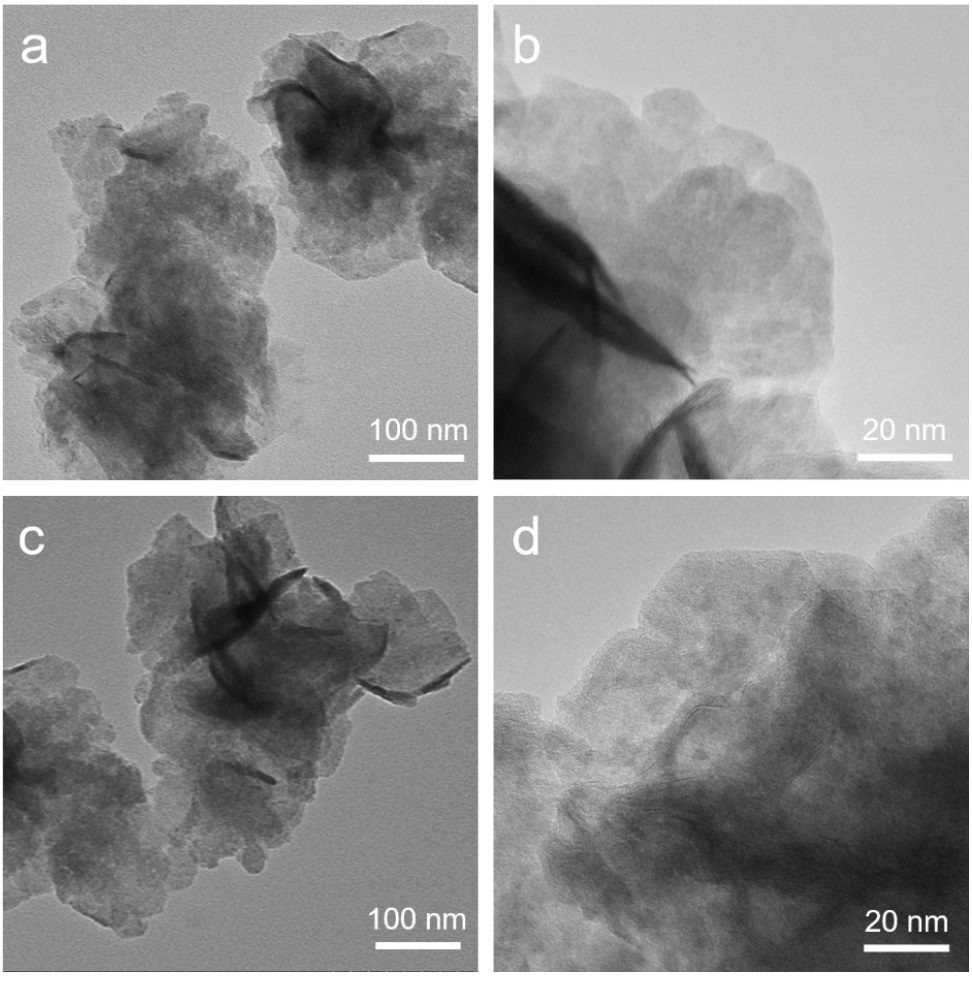

Figure S4. TEM images of MoS_2 nanosheets a-b) before and c-d) after Fe nanodots decoration.

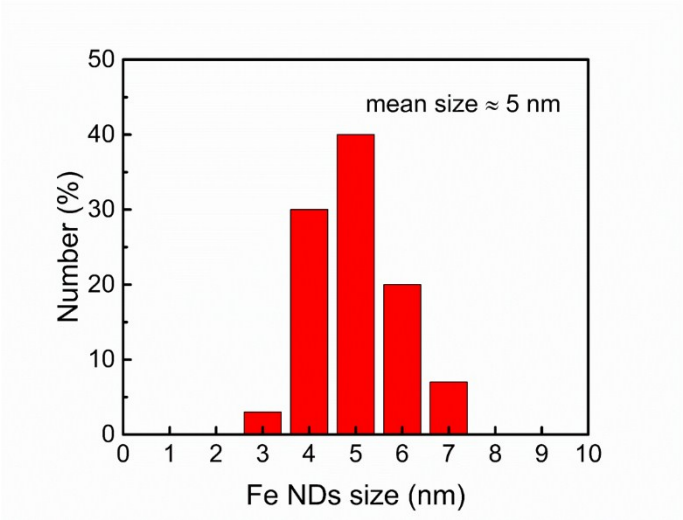

Figure S5. The size distribution histogram of Fe nanodots.

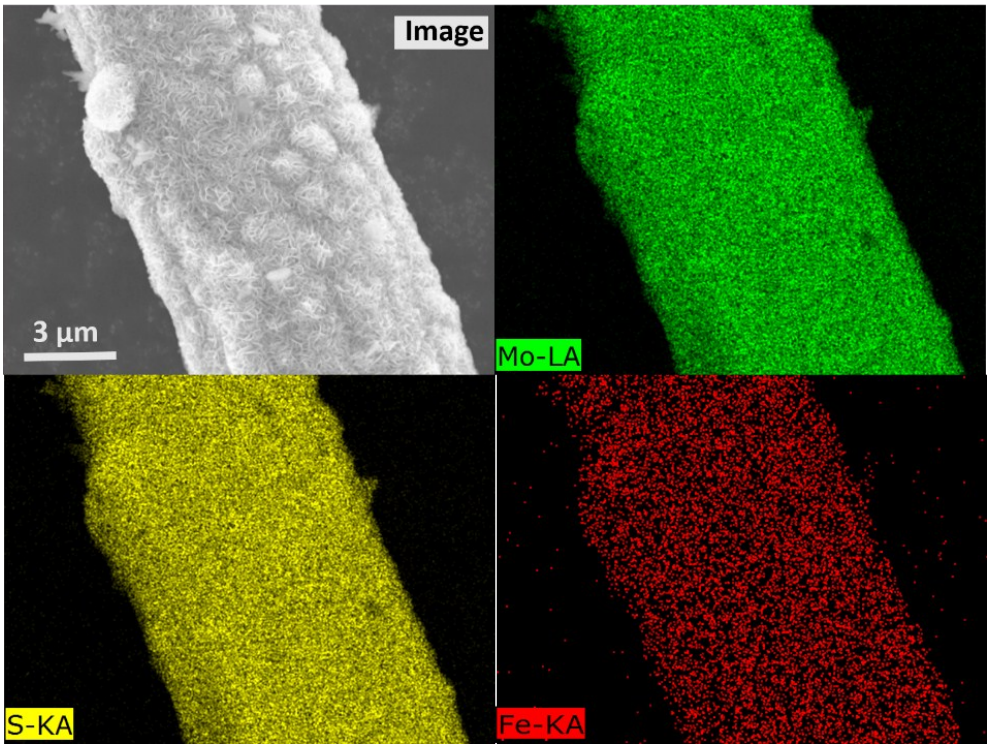

Figure S6. EDS mapping on a single carbon fiber of Fe-MoS_2/CC.

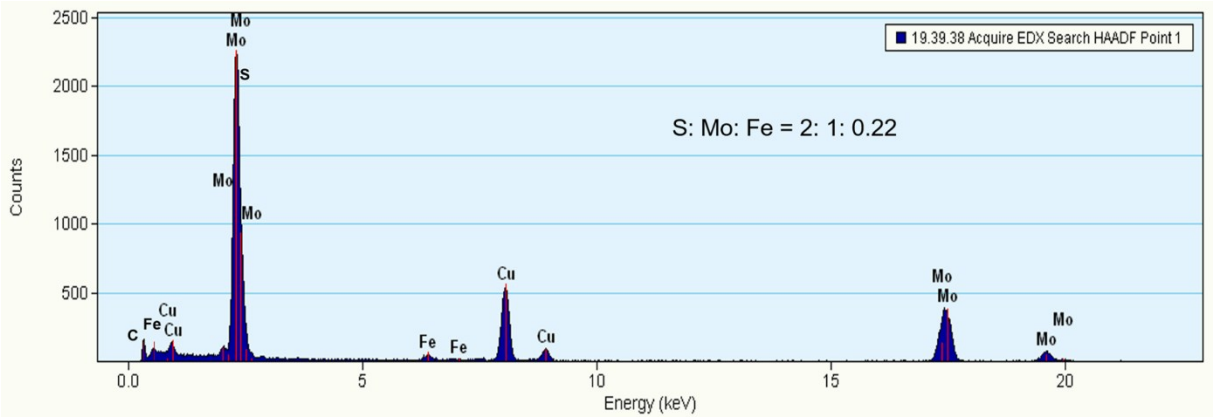

Figure S7. EDS spectrum of Fe-MoS_2. The detected atomic ratio is 2: 1: 0.22 for S: Mo: Fe and the corresponding mass ratio Fe/MoS_2 hybrid is 0.077. The signal of Cu element is ascribed to the copper mesh support for TEM observation. Of note, there is no detectable N signal in Fe-MoS_2 sample within the detection limit of the EDS (~0.5 atomic percent).

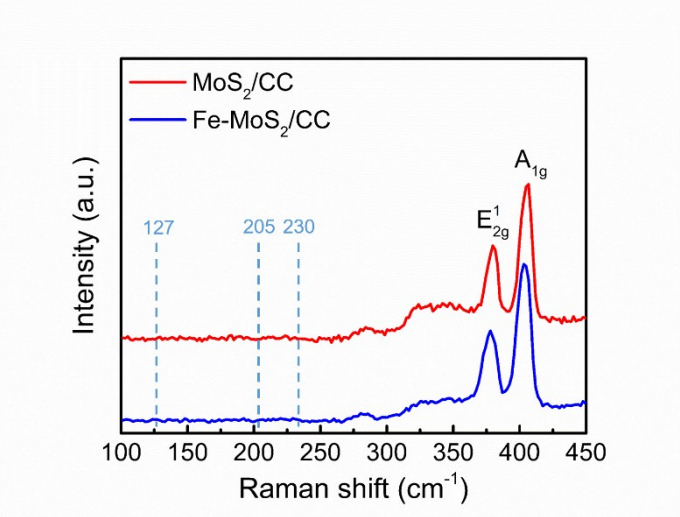

Figure S8. Raman spectra of MoS_2/CC and Fe-MoS_2/CC. Both MoS_2/CC and Fe-MoS_2/CC exhibits two peaks at or around 378.1 cm^{-1} and 403.7 cm^{-1}, attributable to the 2H phase vibrational configurations of the in-plane Mo–S phonon mode (E_{2g}^1) and the out-of-plane Mo-S mode (A_{1g}), respectively. There are no peaks at or around 127 cm^{-1}, 205 cm^{-1} and 230 cm^{-1}, which are associated with the 1T-MoS_2 phonon modes according to the previous sdudy.[8] These results suggest that both MoS_2/CC and Fe-MoS_2/CC are 2H-MoS_2.

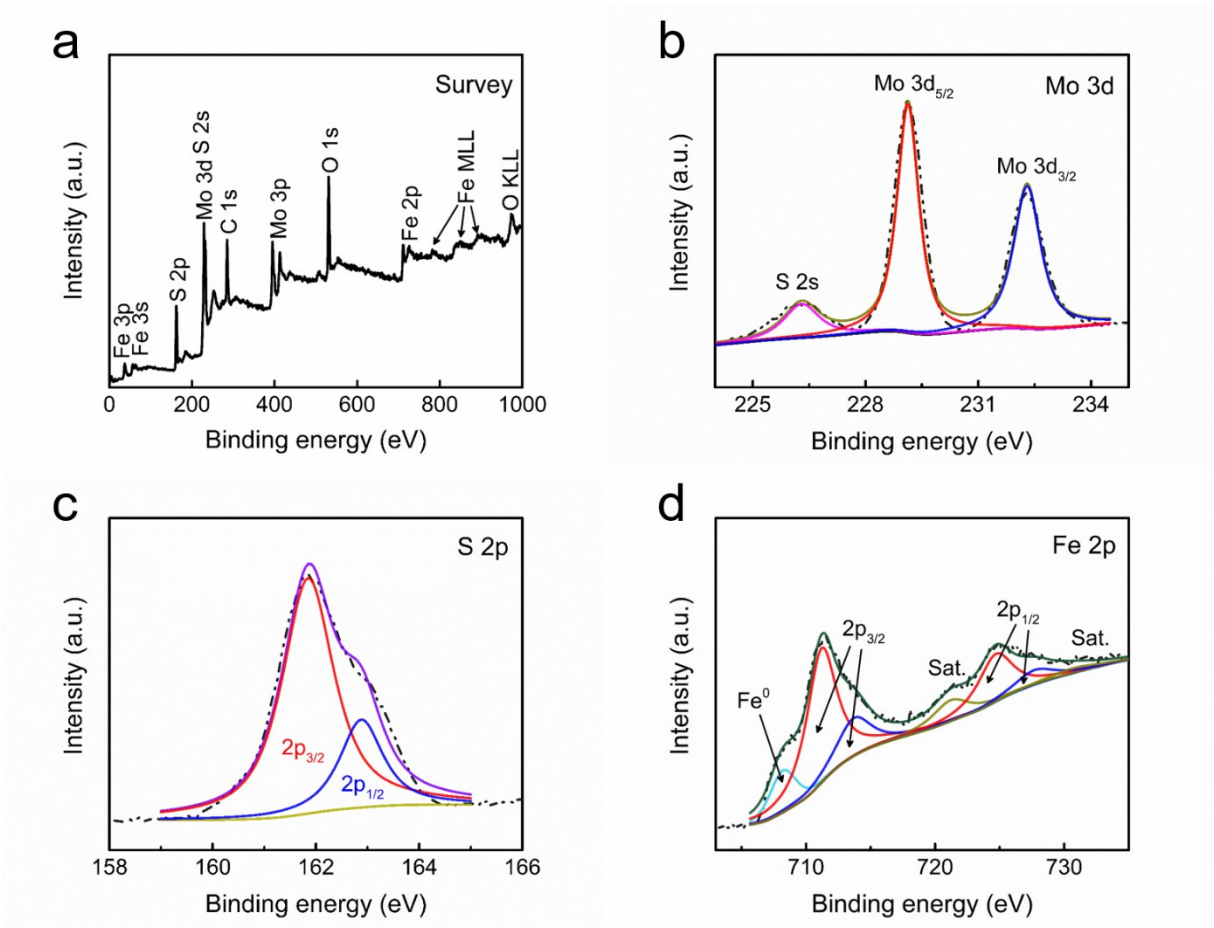

Figure S9. XPS spectra of a) survey, b) Mo 3d, c) S 2p and d) Fe 2p for Fe-MoS_2/CC.

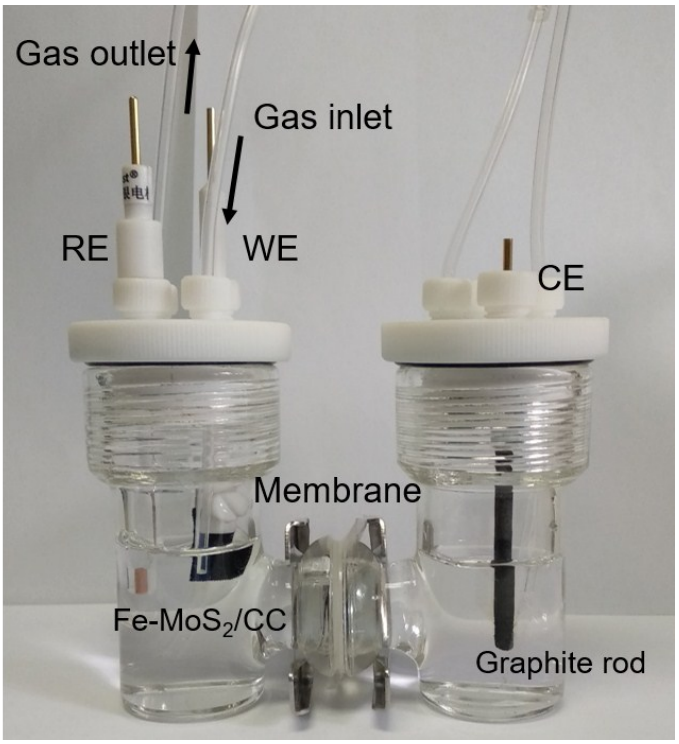

Figure S10. Photograph of the electrochemical cell setup used for the NRR electrolysis.

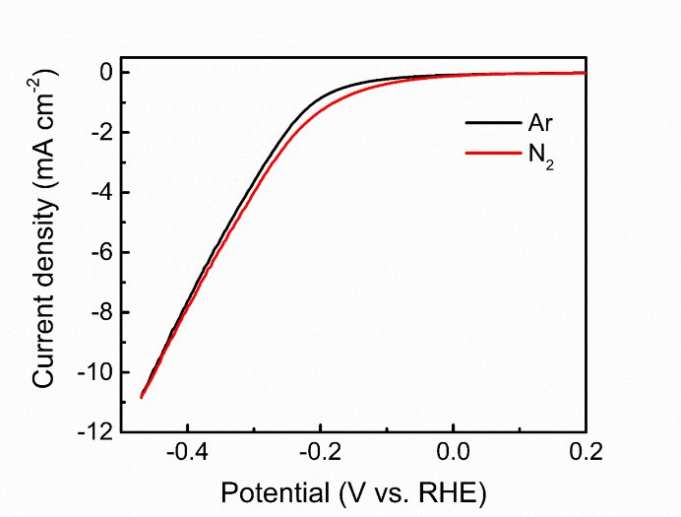

Figure S11. LSV tests of Fe-MoS_2/CC in an Ar- and N_2-saturated 0.1 M KOH aqueous solution under ambient conditions with a scan rate of 5 mV s^{-1}, without current resistance (*iR*) compensation.

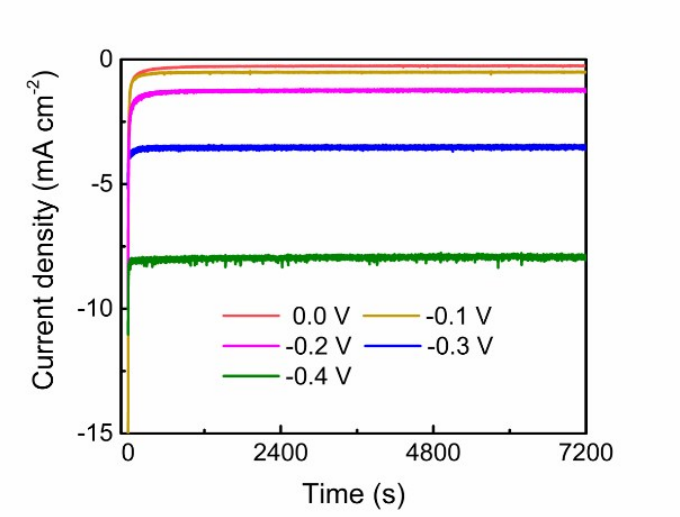

Figure S12. Chronoamperometric results of Fe-MoS_2/CC at the corresponding potentials in N_2-saturated 0.1 M KOH. There is no obvious decline on current density for Fe-MoS_2/CC at various potentials after 2 h electrolysis.

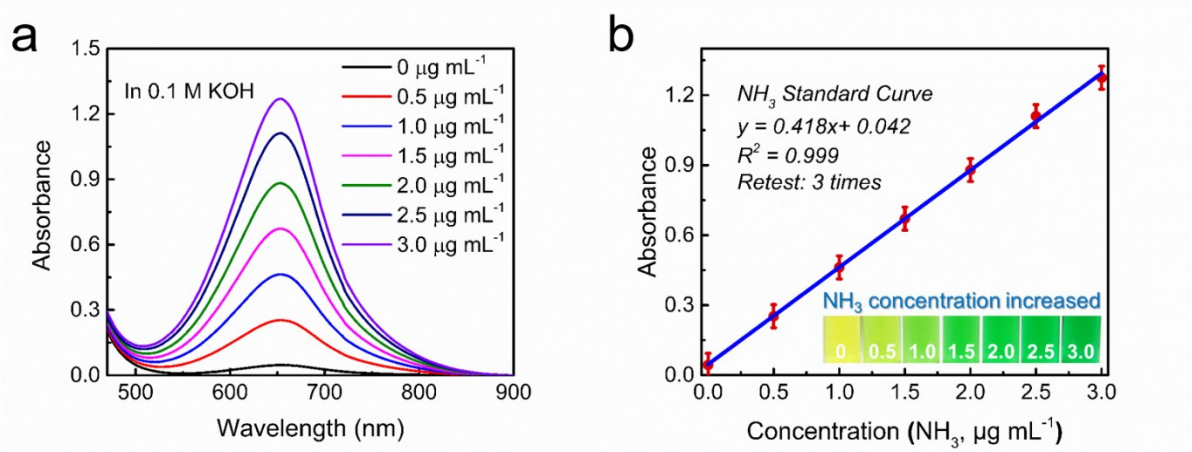

Figure S13. Absolute calibration of the indophenol blue method for estimating NH_3 concentration, using NH_4Cl solutions of known concentration as standards. a) UV-Vis curves of indophenol assays with NH_3 after incubated for 2 hours at room temperature. b) calibration curve used for calculation of NH_3 concentrations. The absorbance at 655 nm was measured by UV-Vis spectrophotometer, and the fitting curve shows good linear relation of absorbance with NH_3 concentration ($y = 0.418x + 0.042$, $R^2 = 0.999$) of three separately independent calibration curves. The inset in b) shows the chromogenic reaction of indophenol indicator with NH_3.

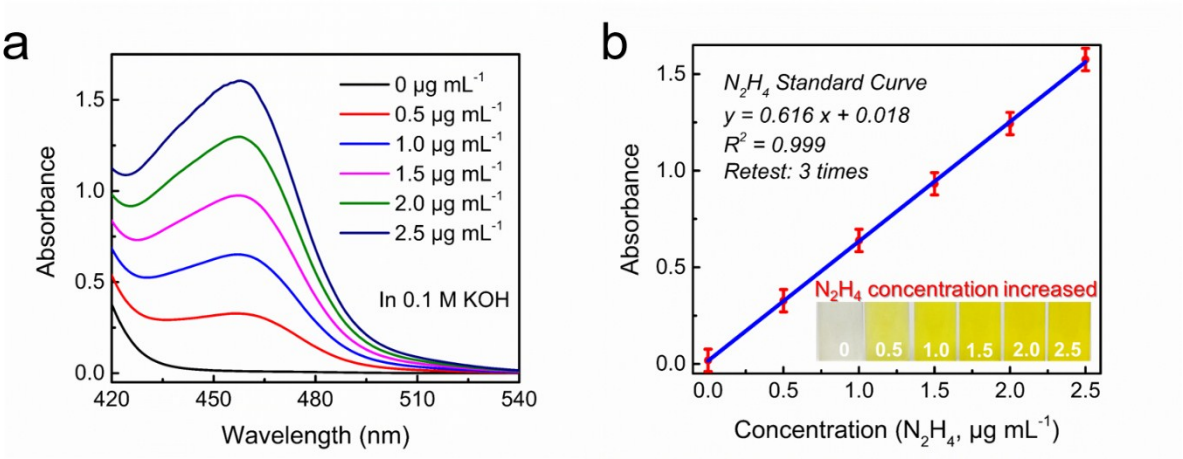

Figure S14. Absolute calibration of the Watt and Chrisp (*p*-dimethylamino-benzaldehyde) method for estimating N_2H_4 concentration, using N_2H_4 solutions of known concentration as standards. a) UV-Vis curves of various N_2H_4 concentration after incubated for 10 min at room temperature. b) calibration curve used for estimation of N_2H_4 concentration. The absorbance at 455 nm was measured by UV-Vis spectrophotometer, and the fitting curve shows good linear relation of absorbance with N_2H_4 concentration ($y = 0.616x + 0.018$, $R^2 = 0.999$) of three times independent calibration curves. The inset in b) shows the chromogenic reaction of *p*-dimethylamino-benzaldehyde indicator with N_2H_4.

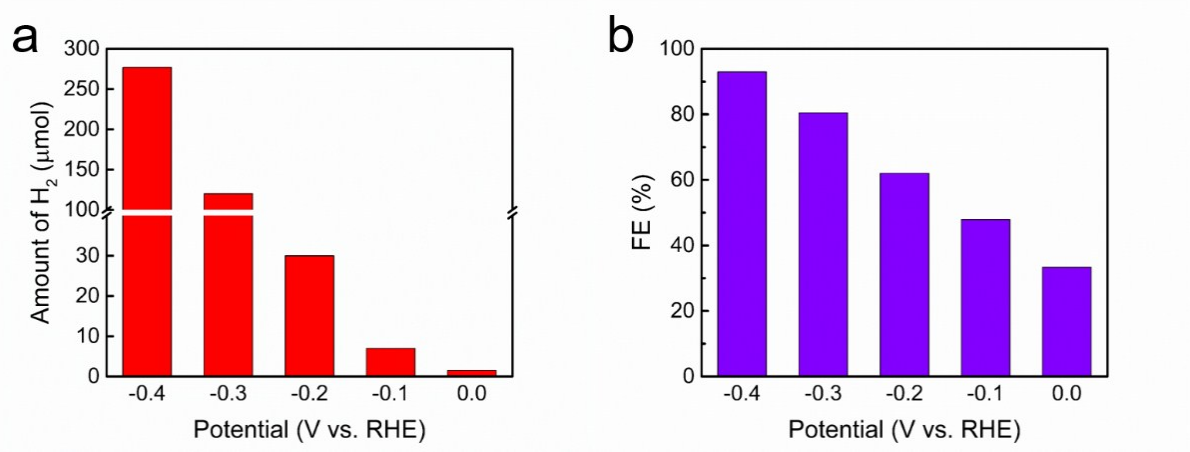

Figure S15. a) Amount of evolved H_2 determined by gas chromatography from the headspace of the cell in N_2-saturated 0.1 M KOH at various potentials. b) The calculated FEs of H_2 formation at various potentials.

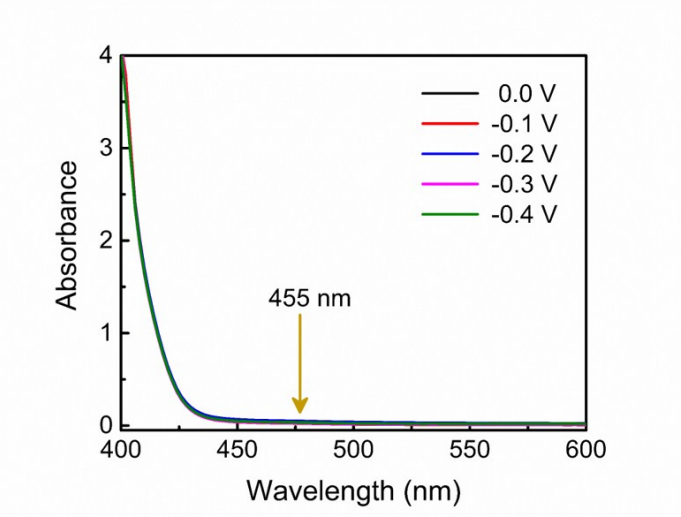

Figure S16. UV-Vis absorption spectra of the electrolytes estimated by the method of Watt and Chrisp after 2-h electrolysis in N_2 atmosphere at each given potential under ambient conditions using Fe-MoS_2/CC as the working electrode. There is no absorbance at 455 nm for the various electrolytes, suggesting no produced N_2H_4 in the solution.

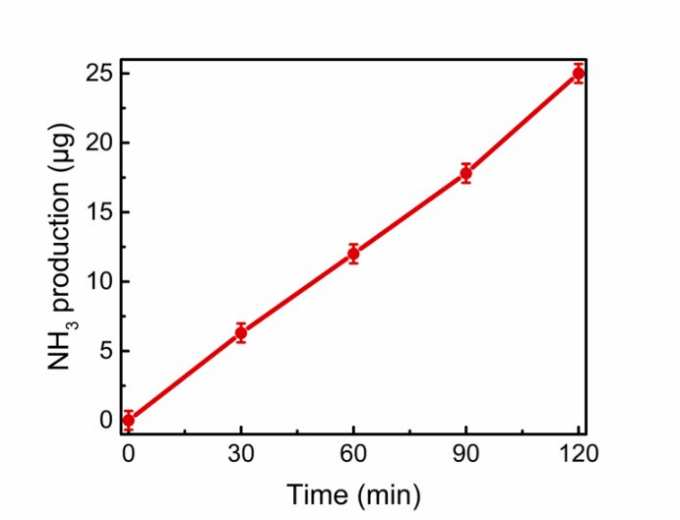

Figure S17. Quantitative determination of NH_3 generated by the as-prepared Fe-MoS_2/CC electrode.

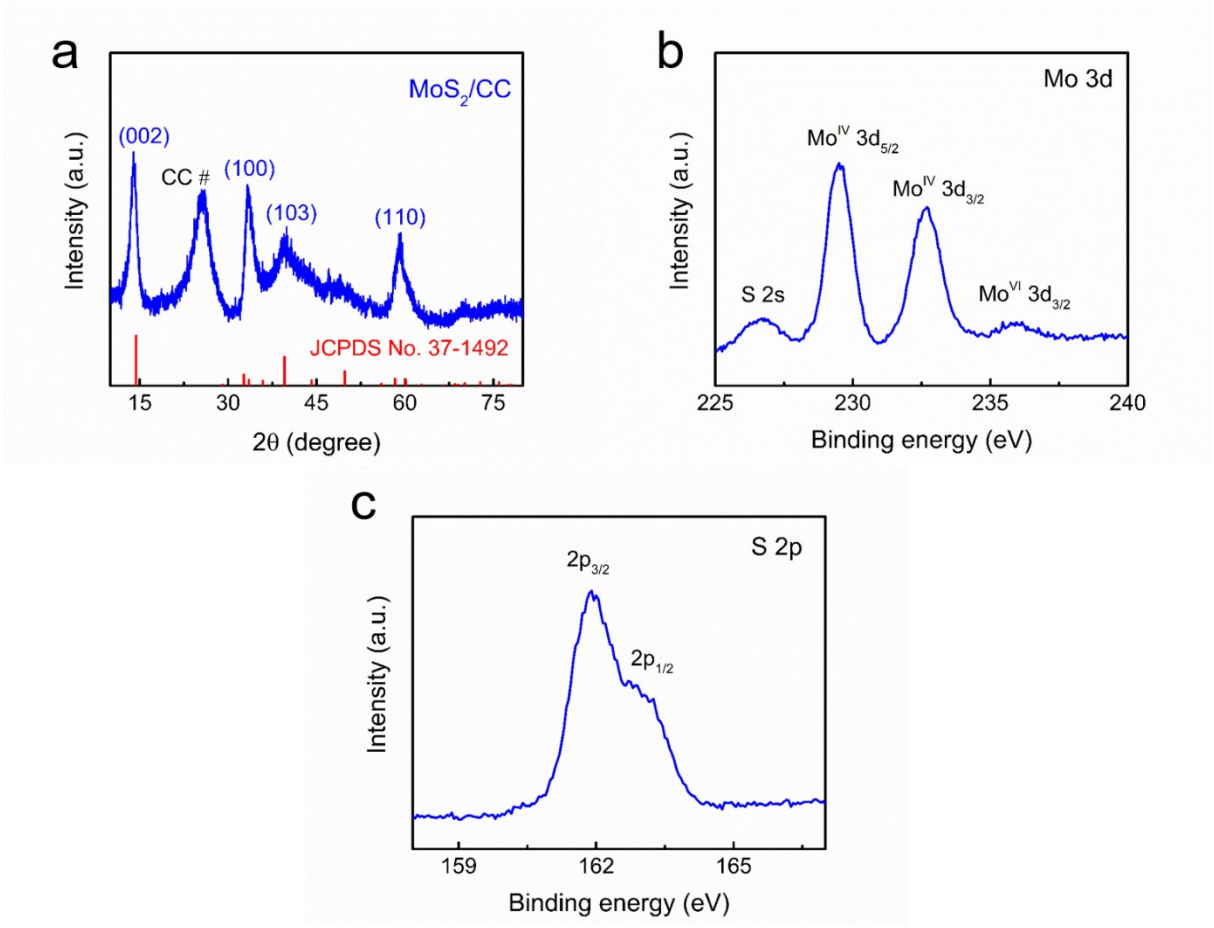

Figure S18. a) XRD pattern of MoS_2/CC. b) Mo 3d and c) S 2p XPS spectra of MoS_2/CC.

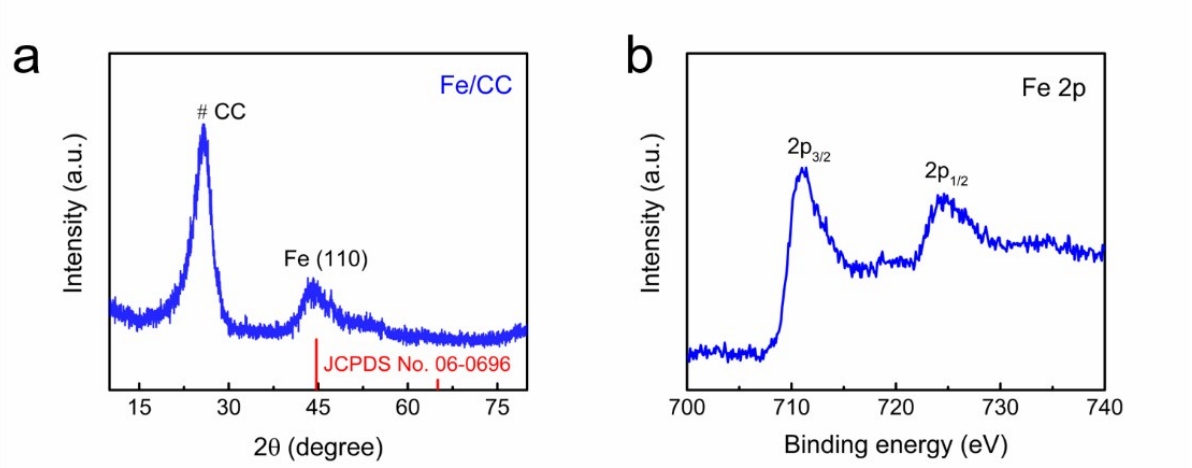

Figure S19. a) XRD pattern of Fe/CC. b) Fe 2p XPS spectrum of Fe/CC.

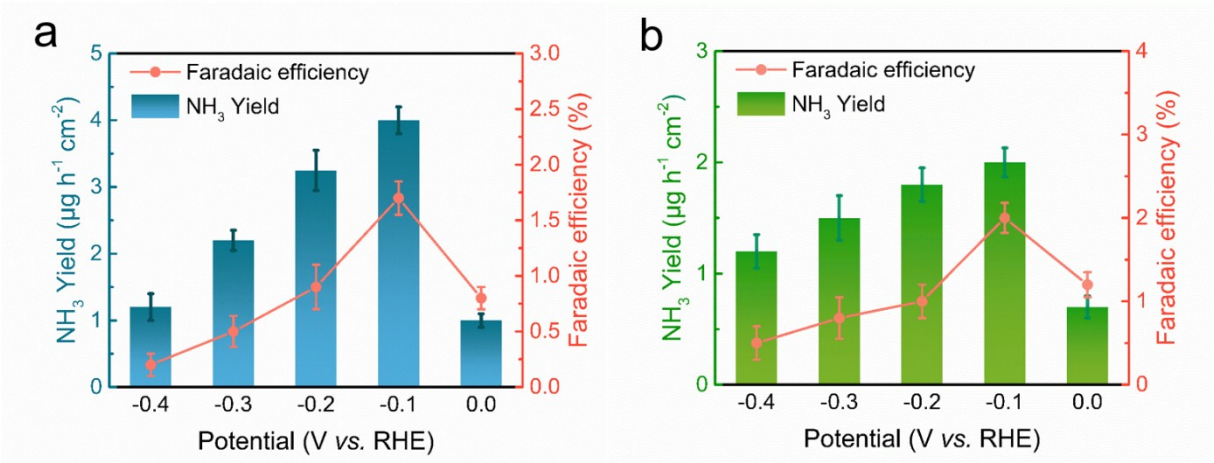

Figure S20. NH_3 yields and Faradaic efficiencies of a) MoS_2/CC, and b) Fe/CC at each given potential.

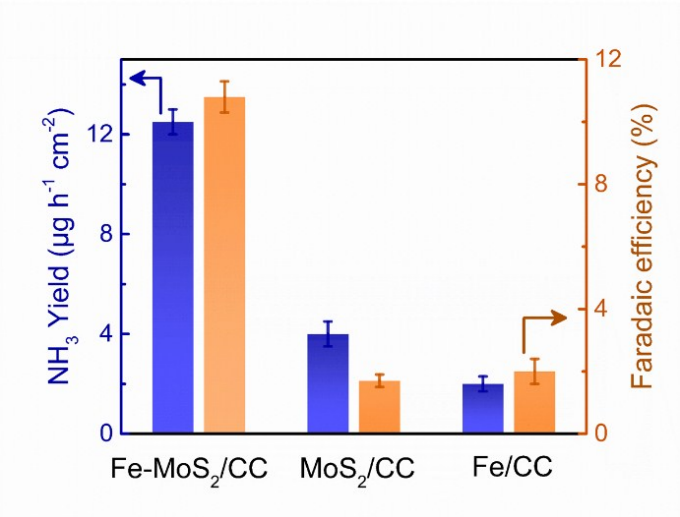

Figure S21. NH_3 yields and Faradaic efficiencies of different electrodes at -0.1 V vs. RHE.

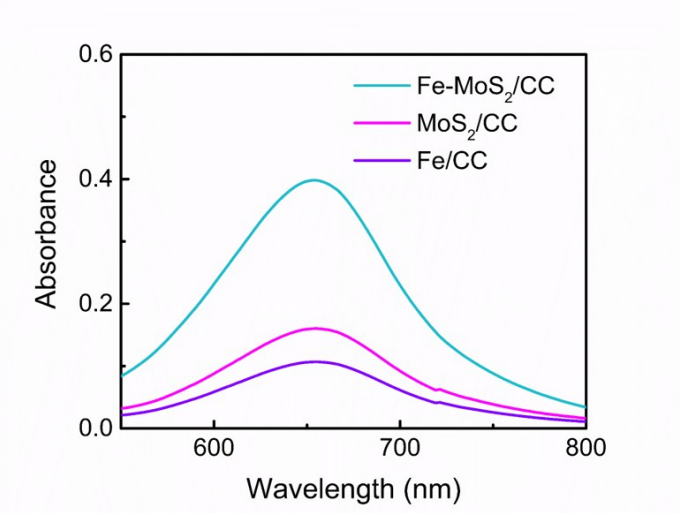

Figure S22. UV-vis absorption spectra of the electrolytes stained with indophenol indicator performed at different electrode samples.

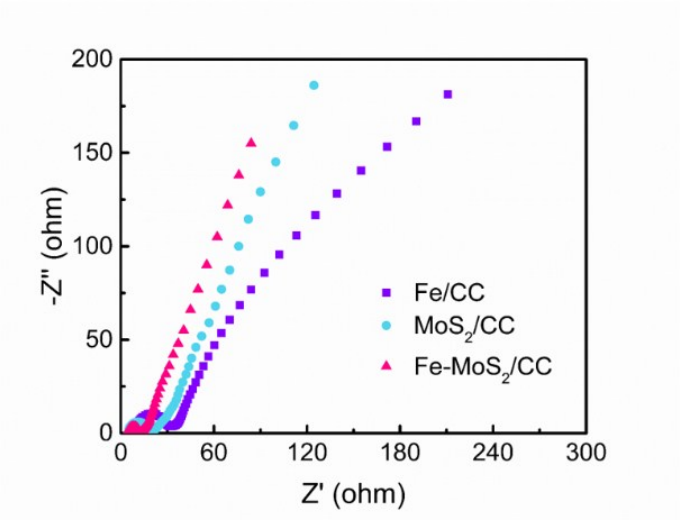

Figure S23. Nyquist plots of Fe/CC, MoS_2/CC and Fe-MoS_2/CC.

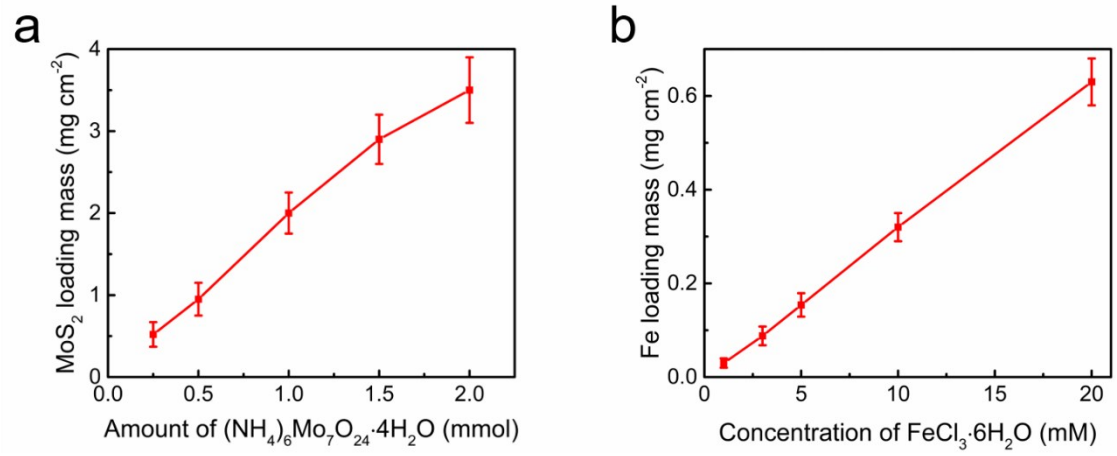

Figure S24. a) The relationship between the concentration of $(NH_4)_6Mo_7O_{24}\cdot 4H_2O$ and the loading of MoS_2; b) The relationship between the concentration of $FeCl_3\cdot 6H_2O$ and the loading of Fe.

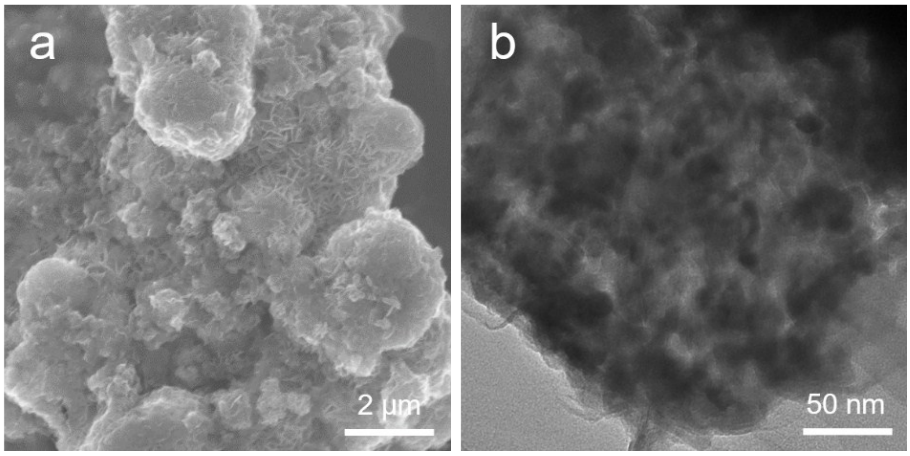

Figure S25. a) SEM and b) TEM images of Fe-MoS_2/CC with high Fe loading (mass ratio of Fe/MoS_2 is 0.321). The hierarchical structure of MoS_2 nanosheets is quenched by the high content of Fe loading.

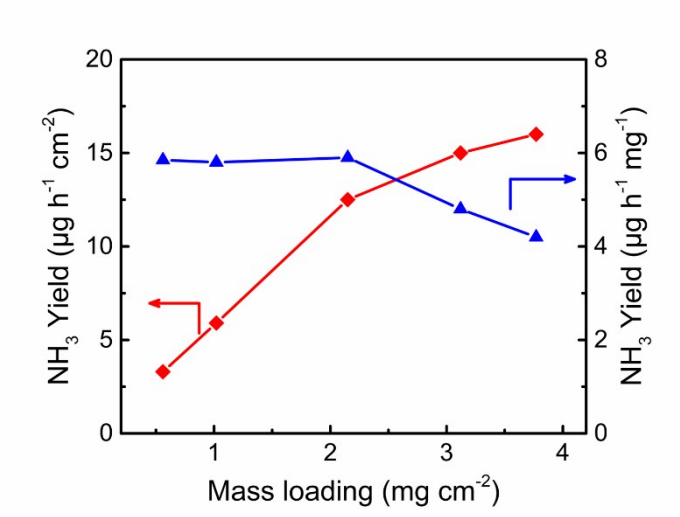

Figure S26. NH_3 yields Fe-MoS_2/CC with different mass loadings (the mass ratio of Fe/MoS_2 is kept 0.077): area catalytic activity (red line); mass catalytic activity (blue line). This figure shows the area catalytic activity and mass catalytic activity of the Fe-MoS_2/CC electrode with catalyst loadings of 0.56, 1.02, 2.15, 3.12 and 3.77 mg cm^{-2}. The mass catalytic activities of the last two loadings have shown significantly decline due to the increasing thickness of the catalyst layer over the substrate electrode, namely the self-masking of catalytically active sites. This could have forbidden the catalysts to achieve the same specific activities as that of the ones with the lower loadings. According to the above results, the NH_3 yields with various mass loadings of Fe-MoS_2/CC suggest 2.15 mg cm^{-2} is the optimal loading.

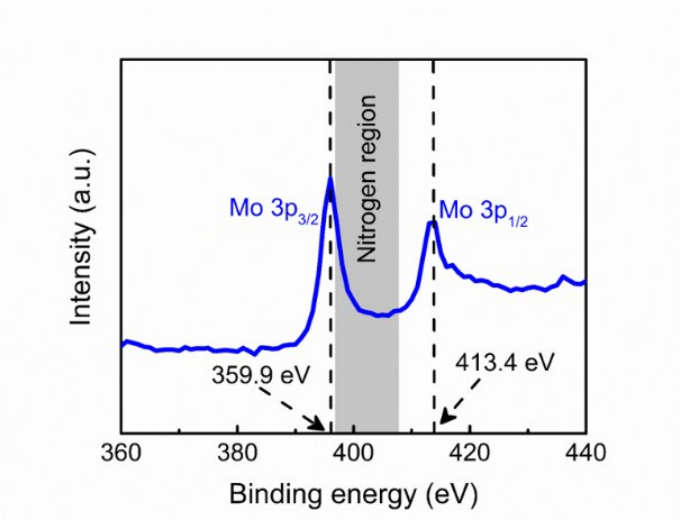

Figure S27. High resolution XPS spectrum around nitrogen region. Obviously, there is no signal peak in the nitrogen region (397.0-407.2 eV), indicating no N species in the Fe-MoS_2/CC sample. The binding energy at 359.9 eV and 413.4 eV belong to Mo $3p_{3/2}$ and Mo $3p_{1/2}$, respectively.

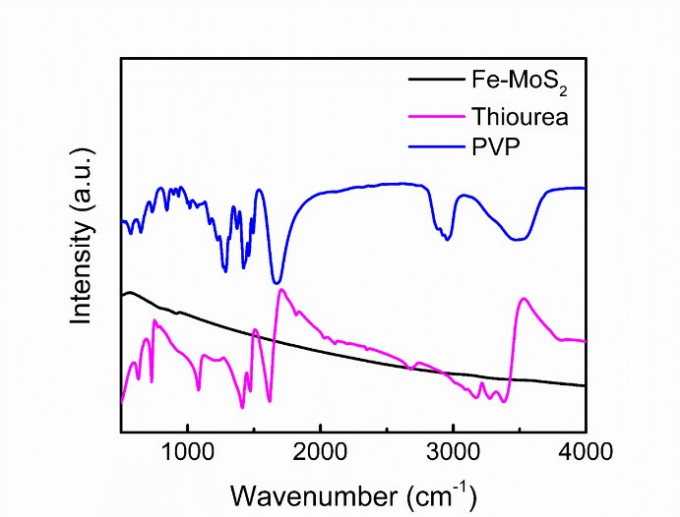

Figure S28. FTIR spectra of pure thiourea, PVP and Fe-MoS_2 sample.

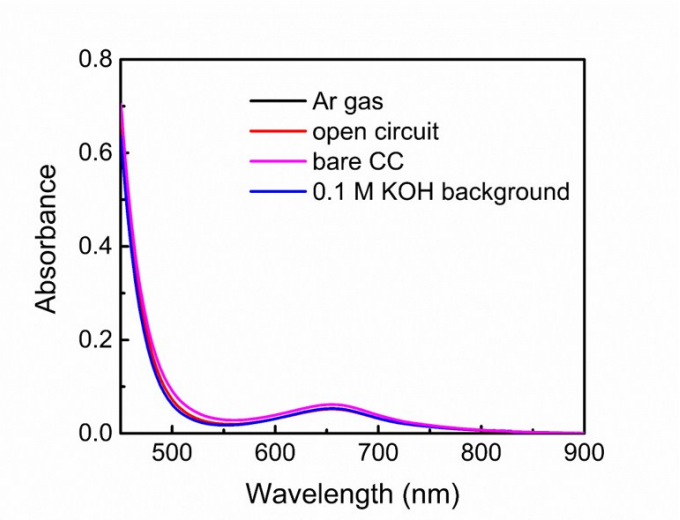

Figure S29. UV/Vis absorption spectra of the electrolyte stained with indophenol indicator. i) Ar gas flow was supplied at −0.1 V vs. RHE for 2 h; ii) N_2 gas flow was bubbled into the cell at open-circuit for 2 h; iii) the bare CC electrode without Fe-MoS_2 catalyst was served as the working electrodes; iv) only 0.1 M KOH electrolyte without Ar/N_2 gas or applied voltage.

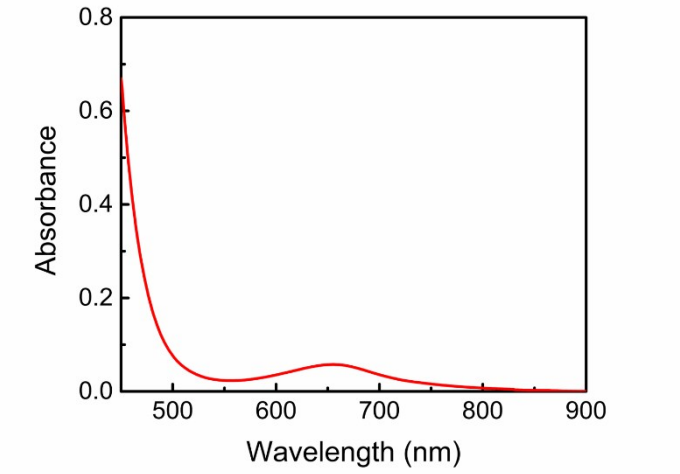

Figure S30. UV-Vis absorption spectra of the electrolyte (Ar control experiment after NRR test) stained with indophenol indicator.

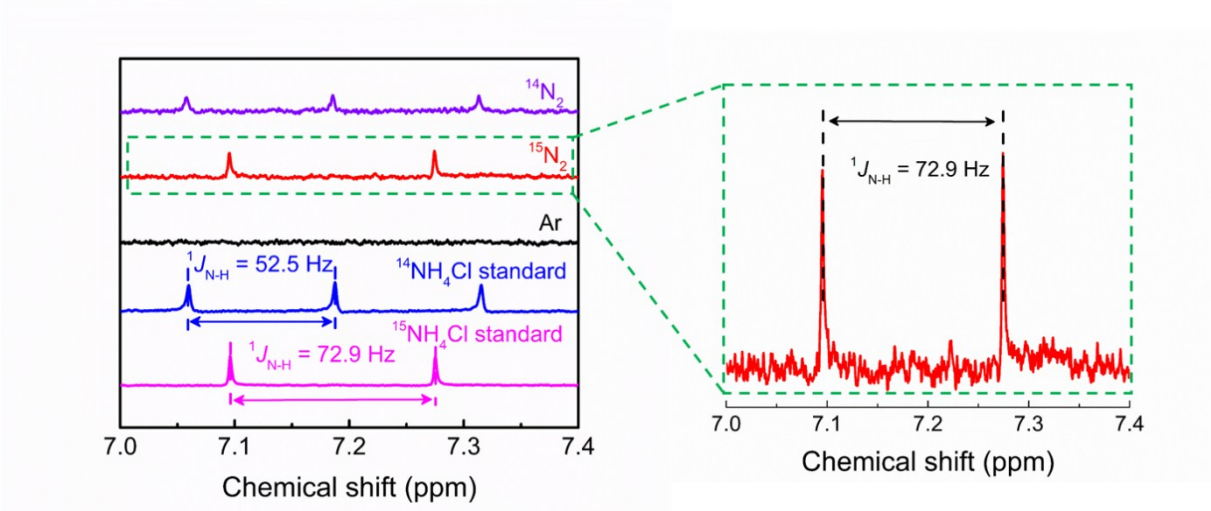

Figure S31. ^1H NMR analysis of the electrolyte fed by $^{14}N_2$ and $^{15}N_2$ after electrolytic reaction. A triplet coupling for $^{14}NH_4^+$ and a doublet coupling for $^{15}NH_4^+$ in the ^1H NMR spectra are used to distinguish them. The results show that only $^{15}NH_4^+$ was detected in the electrolyte when $^{15}N_2$ was supplied as the feeding gas, and no NH_4^+ was detected when Ar gas was supplied, which are consistent with the control experiments and confirm that the NH_3 was produced by electroreduction of N_2.

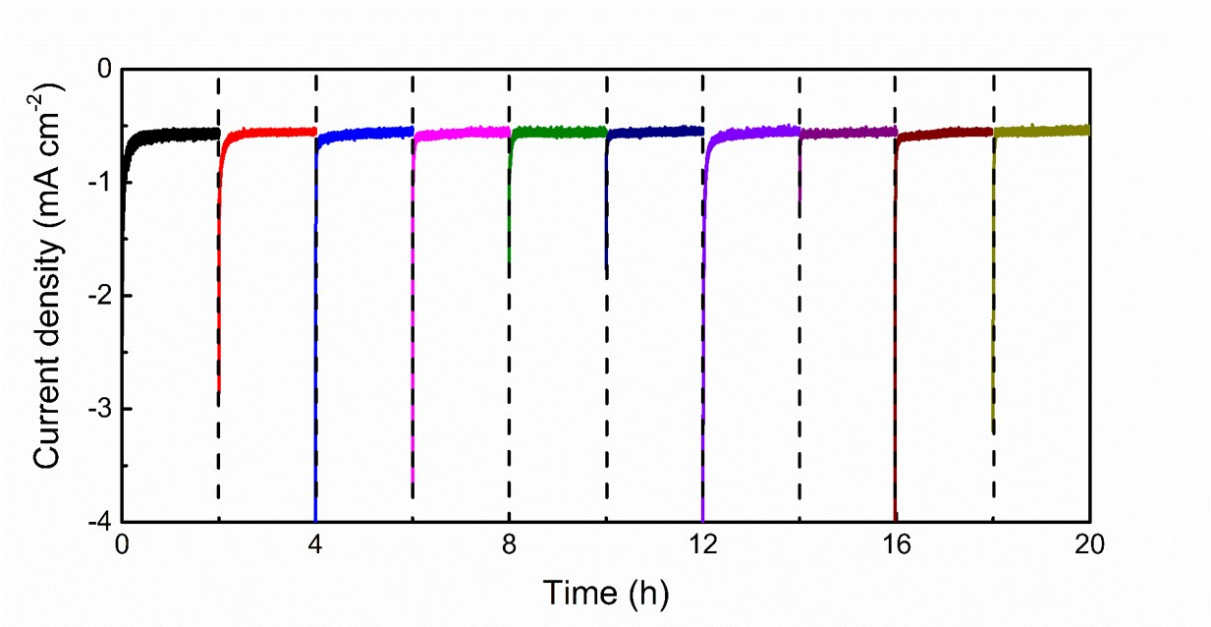

Figure S32. Chronoamperometric results of the Fe-MoS_2/CC in N_2-saturated 0.1 M KOH electrolyte at −0.1 V vs. RHE under ten consecutive recycling electrolysis.

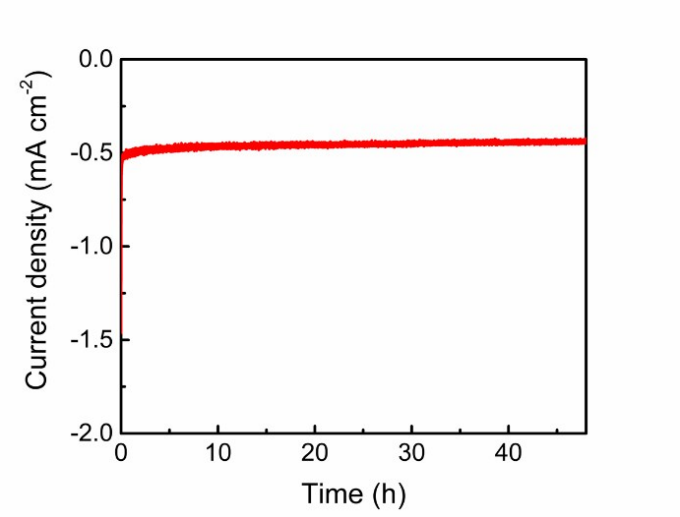

Figure S33. Chronoamperometric curve of Fe-MoS_2/CC in N_2-saturated 0.1 M KOH electrolyte at −0.1 V vs. RHE for continuous 48 h.

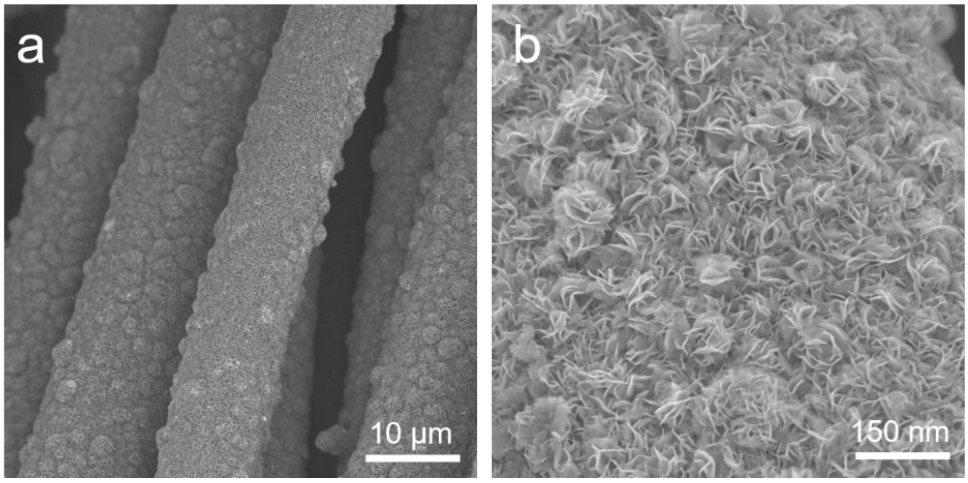

Figure S34. SEM images for Fe-MoS_2/CC after long-time stability test. The Fe-MoS_2 hybrids are still attached closely on CC support without peeling off from the substrate. The hierarchical structures of the samples are still maintained.

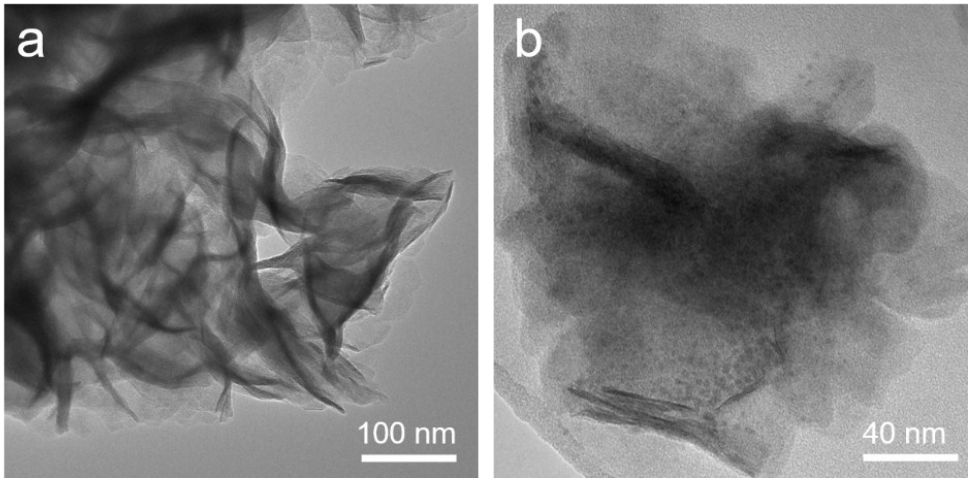

Figure S35. TEM images for Fe-MoS_2/CC after long-time stability test. MoS_2 nanosheets still hold the regular wrinkles and corrugations, with uniformly distributed Fe nanodots on their surface.

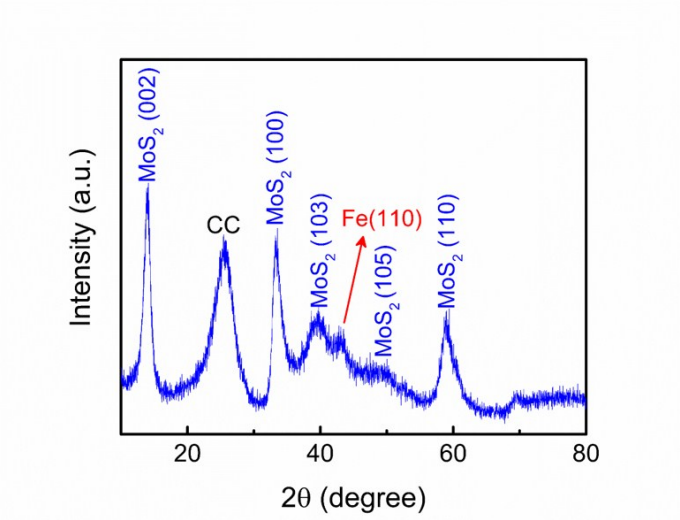

Figure S36. XRD pattern for Fe-MoS_2/CC after long-time stability test.

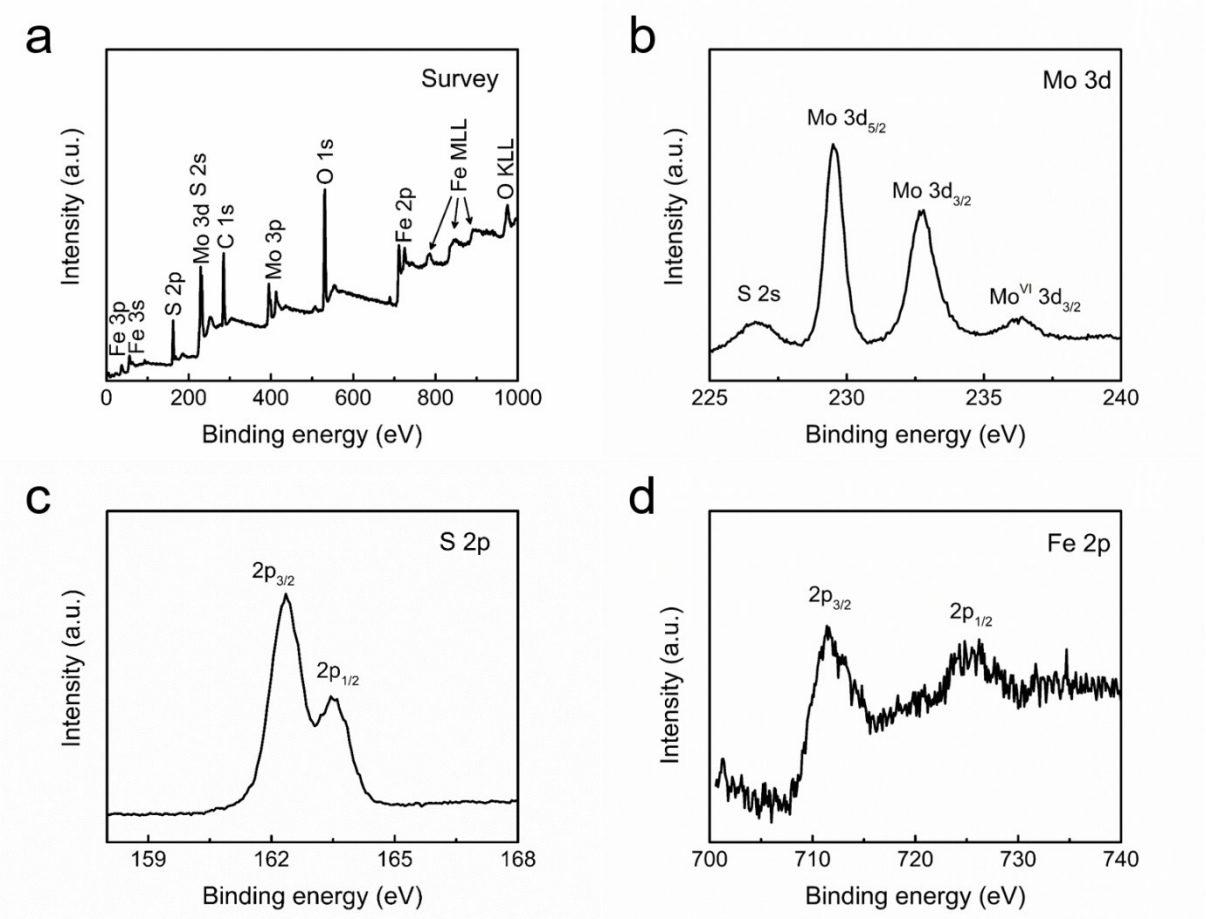

Figure S37. a) Survey, b) Mo 3d, c) S 2p, and d) Fe 2p XPS spectra for Fe-MoS_2/CC after long-time stability test. According to the XPS results, the mass ratio of Fe/MoS_2 in Fe-MoS_2/CC is 0.076.

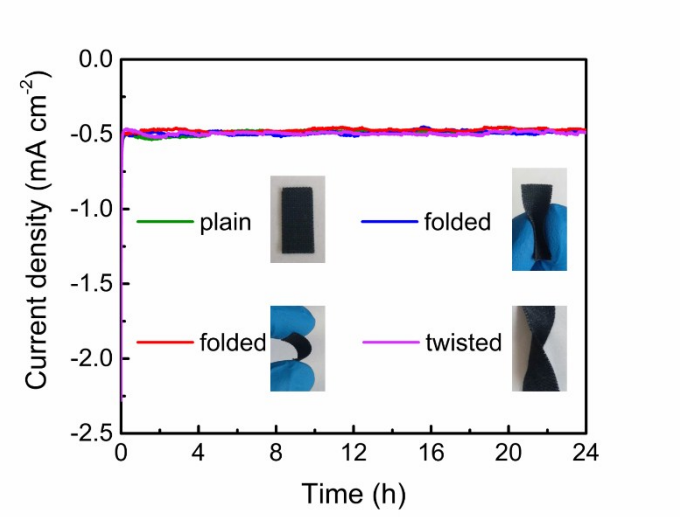

Figure S38. Chronoamperometric curves of Fe-MoS_2/CC at -0.1 V vs. RHE for continuous 24 h electrolysis after folding or twisting ten times.

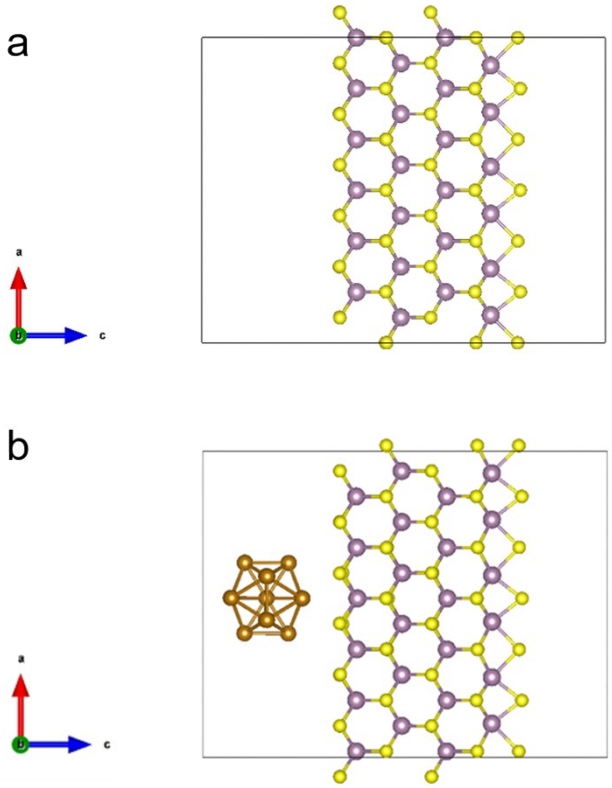

Figure S39. The theoretical models of top view of a) MoS_2 and b) Fe-MoS_2 used in DFT calculations. Mo atoms: purple, S atoms: yellow, Fe atoms: brown.

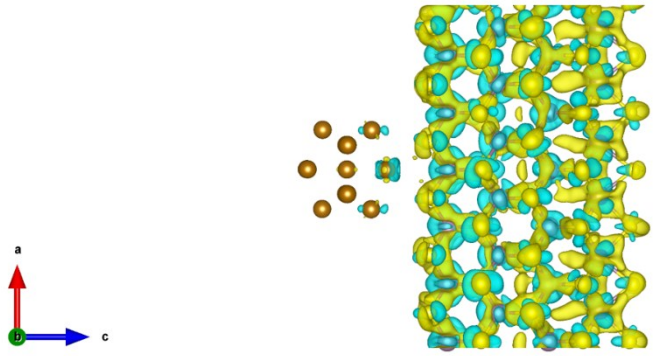

Figure S40. Differential charge density of the Fe-MoS_2 hybrid. Yellow and cyan colors represent electron-rich and electron-defective regions, respectively.

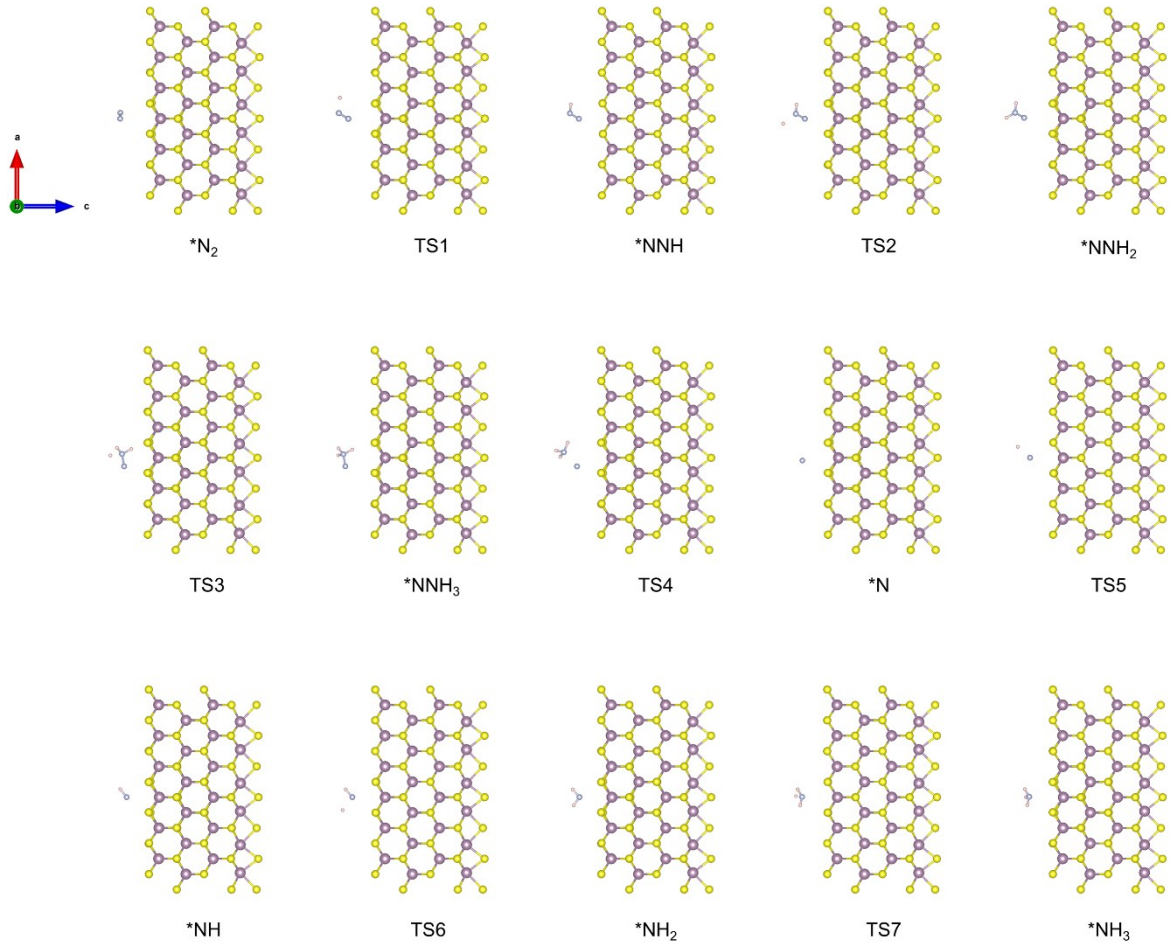

Figure S41. The adsorption structures of the intermediate and transition states (TS) on MoS_2 catalyst. Mo atoms: purple, S atoms: yellow.

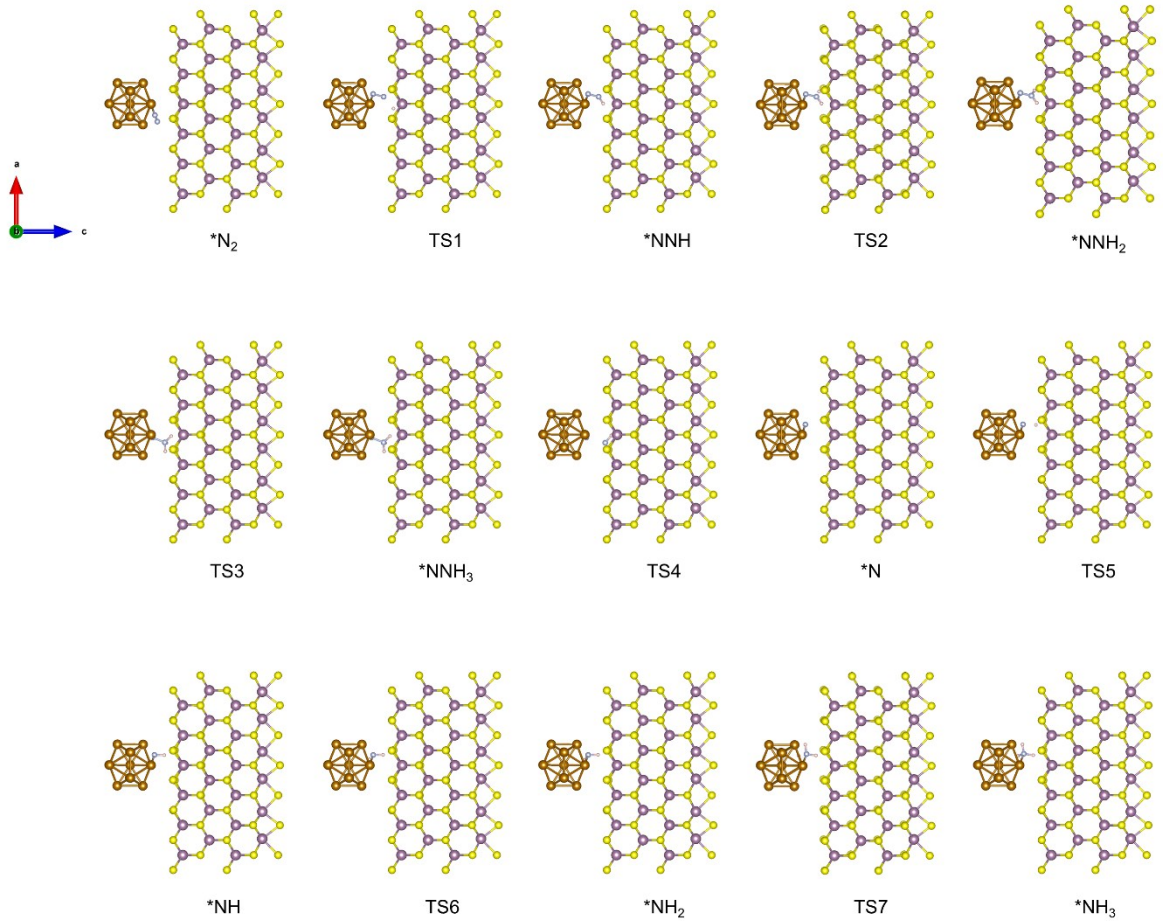

Figure S42. The adsorption structures of the intermediate and transition states (TS) on Fe-MoS_2 catalyst. Mo atoms: purple, S atoms: yellow, Fe atoms: brown.

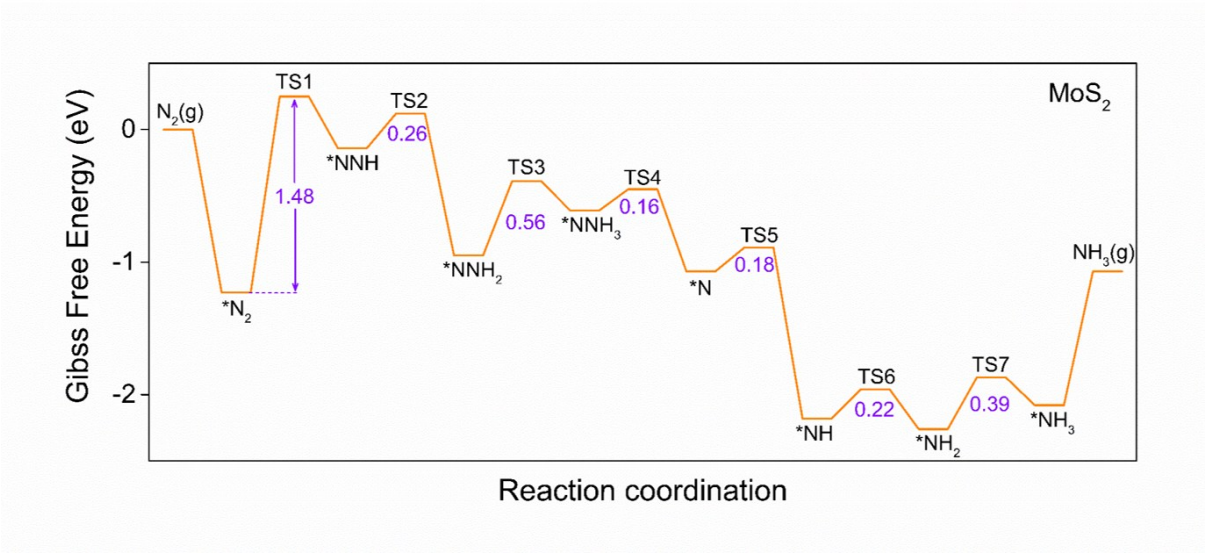

Figure S43. Free-energy diagram of NRR for MoS_2 when there is no applied bias (U = 0 V). Note: "*" denotes adsorbed species. The value in the Figure represents the activation barrier for elementary step.

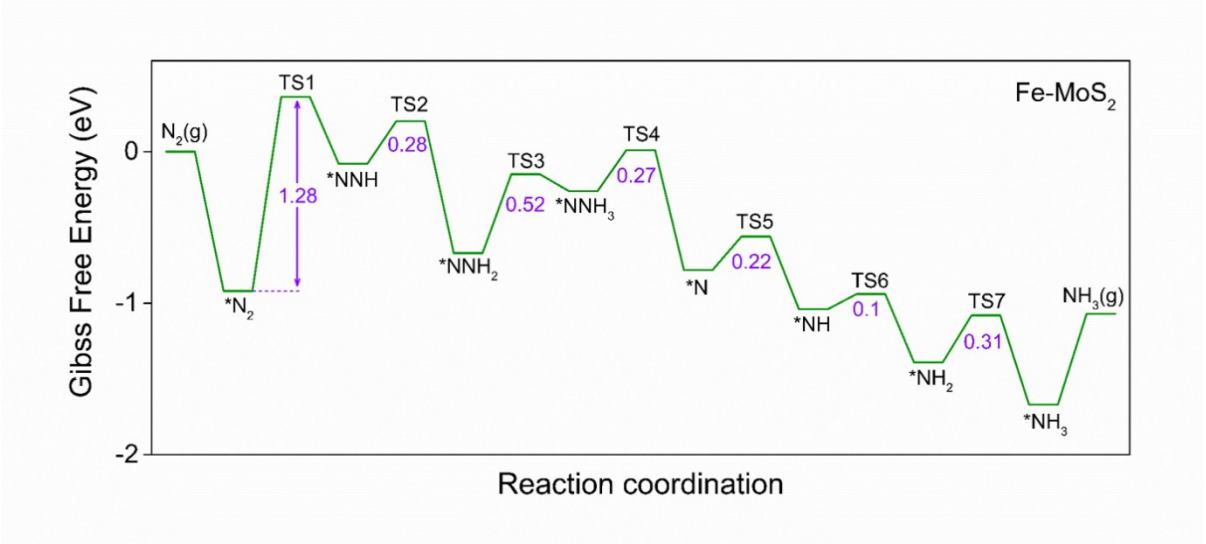

Figure S44. Free-energy diagram of NRR for Fe-MoS_2 when there is no applied bias (U = 0 V). Note: "*" denotes adsorbed species. The value in the Figure represents the activation barrier for elementary step.

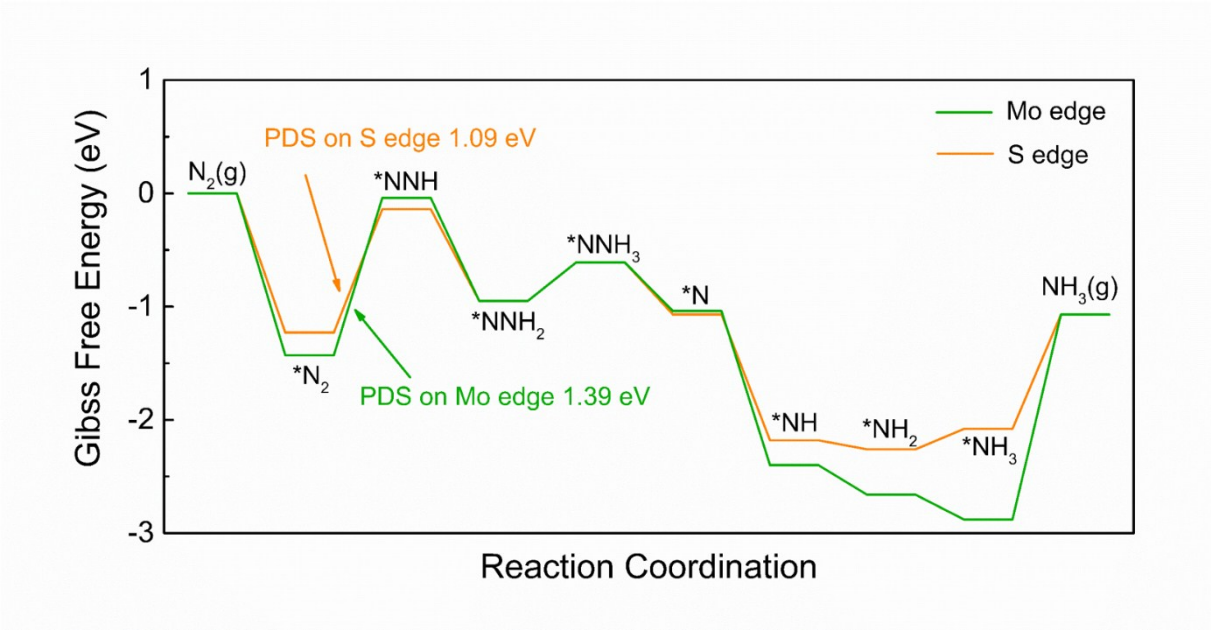

Figure S45. Free-energy diagram of NRR on Mo edge and S edge for MoS_2 when there is no applied bias (U = 0 V). Note: "*" denotes adsorbed species.

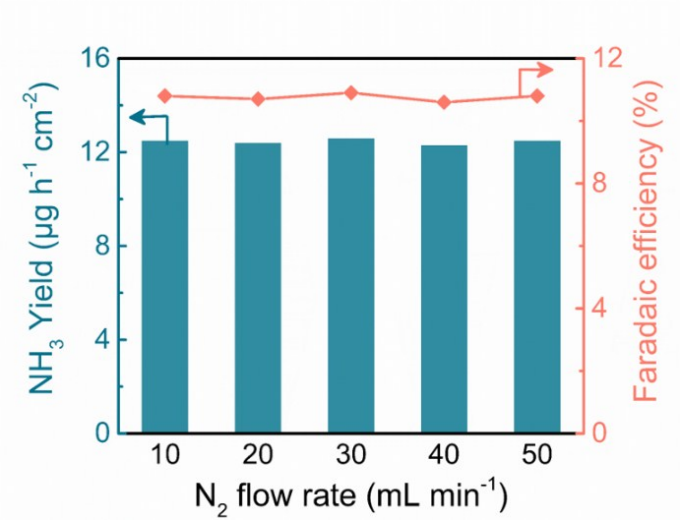

Figure S46. Yield rates of NH_3 and FEs under different N_2 flow rate at −0.1 V vs. RHE. All experiments were carried out in 0.1 M KOH under conditions.

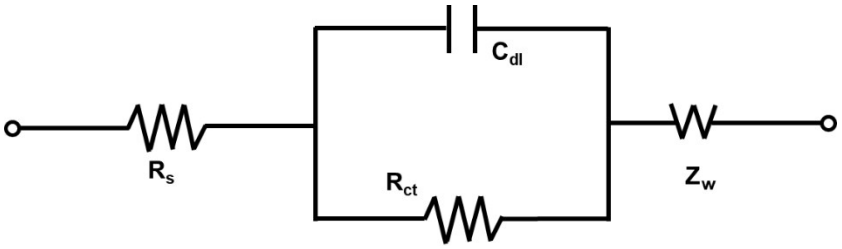

Figure S47. Randles' equivalent circuit used for fitting impedance spectra. R_s, C_{dl}, R_{ct}, and Z_w stand for the solution resistance, double-layer capacitance, charge transfer resistance, and finite length Warburg impedance element, respectively.

Table S1. The Faradaic efficiency of Fe-MoS_2/CC predicted from LSV measurements.

Potential (V vs. RHE)	0	-0.1	-0.2	-0.3	-0.4
FE	27.3%	42.1%	33.1%	8.9%	3.0%

These values are in line with the trend of the FEs during constant potential electrolysis (as quantified by colorimetry, Figure 3a), although the FEs predicted from LSV measurements are higher than that obtained from constant potential electrolysis.

Table S2. Comparison of the NRR performance of the Fe-MoS_2/CC with other catalysts reported to date under ambient conditions (room temperature and atmospheric pressure).

Catalyst	Electrolyte	Potential (V vs. RHE)	NH_3 yield rate	Faradaic efficiency	Reference
Fe-MoS_2/CC	0.1 M KOH	-0.1	12.5 μg h^{-1} cm^{-2}	10.8 %	This work
PEBCD/C	0.5 M Li_2SO_4	−0.5	1.58 μg h^{-1} cm^{-2}	2.85 %	*J. Am. Chem. Soc.* **2017**, *139*, 9771-9774
a-Au/CeO_x–RGO	0.1 M HCl	-0.2	8.3 μg h^{-1} mg^{-1}	10.10 %	*Adv. Mater.* **2017**, *29*, 1700001
Au nanorod	0.1 M KOH	−0.2	1.648 μg h^{-1} cm^{-2}	3.88 %	*Adv. Mater.* **2017**, *29*, 1604799
Fe_2O_3/CNT	$KHCO_3$	−2.0 (vs. Ag/AgCl)	0.22 μg h^{-1} cm^{-2}	<0.05 %	*Angew. Chem. Int. Ed.* **2017**, *56*, 2699-2703
MoS_2/CC	0.1 M Na_2SO_4	-0.5	8.08×10^{-11} mol s^{-1} cm^{-2} (4.94 μg h^{-1} cm^{-2})	1.17 %	*Adv. Mater.* **2018**, *30*, 1800191

Boron-doped graphene	0.05 M H_2SO_4	-0.5	9.8 μg h^{-1} cm^{-2}	10.8%	*Joule* **2018**, *2*, 1610-1622
Pd/C	0.1 M PBS	+0.1	4.5 μg h^{-1} mg^{-1}	8.2 %	*Nat Commun.* **2018**, *9*, 1795
polymeric carbon nitride	0.1 M HCl	-0.2	8.09 μg h^{-1} mg^{-1}	11.59 %	*Angew. Chem. Int. Ed.* **2018**, *57*, 10246
ZIF-derived carbon	0.1 M KOH	-0.3	3.4×10^{-6} mol h^{-1} cm^{-2} (57.8 μg h^{-1} cm^{-2})	10.2 %	*Nano Energy* **2018**, *48*, 217-226
VN/CC	0.1 M HCl	-0.3	2.48×10^{-10} mol^{-1} s^{-1} cm^{-2} (15.2 μg h^{-1} cm^{-2})	3.58 %	*Chem. Commun.* **2018**, *54*, 5323-5325
Au hollow nanocages	0.5 M $LiClO_4$	-0.4	3.74 μg h^{-1} cm^{-2}	35.9 %	*J. Phys. Chem. Lett* **2018**, *9*, 5160-5166
MoO_3	0.1 M HCl	-0.4	4.80×10^{-10} mol^{-1} s^{-1} cm^{-2} (29.43 μg h^{-1} cm^{-2})	1.9 %	*J. Mater. Chem. A*, **2018**, *6*, 12974-12977
Ru NPs	0.01 M HCl	+0.01	2.00 mg h^{-1} m^{-2} (20.0 μg h^{-1} cm^{-2})	5.4%	*ChemSusChem* **2018**, *11*, 3416 -3422
MXene/SSM	0.5 M Li_2SO_4	-0.1	4.72 μg h^{-1} cm^{-2}	4.62%	*Joule* **2019**, *3*, 279-289
MnO/TM	0.1 M Na_2SO_4	-0.39	6.72 μg h^{-1} cm^{-2}	8.02%	*Adv. Sci.* **2019**, *6*, 1801182
Ru/2H-MoS_2	0.01 M HCl	-0.15	0.91×10^{-10} mol cm^{-2} s^{-1} (5.6 μg h^{-1} cm^{-2})	12.2%	*ACS Energy Lett.* **2019**, *4*, 430-435
PdRu TPs	0.1 M KOH	-0.2	11.9 μg h^{-1} cm^{-2}	1.85%	*J. Mater. Chem. A,* **2019**,*7*, 801-805

Table S3. The reaction energy (eV) of different intermediates, where the * denotes the adsorption site on the catalyst.

Intermediate	Fe-MoS_2	MoS_2
N_2 - $*N_2$	-0.92	-1.23
$*N_2$ - *NNH	0.84	1.09
*NNH - $*NNH_2$	-0.59	-0.81
$*NNH_2$ - $*NNH_3$	0.41	0.34
$*NNH_3$ - *N	-0.52	-0.46
*N - *NH	-0.26	-1.11
*NH - $*NH_2$	-0.35	-0.08
$*NH_2$ - $*NH_3$	-0.28	0.18
$*NH_3$ - NH_3	0.6	1.01

Table S4. The DFT Calculated zero point energies E_{ZPE} and *TS* of different intermediates, where the * denotes the adsorption site on the MoS_2 catalyst.

Intermediate	E_{ZPE} (eV)	*TS* (eV)
$*N_2$	0.21	0.08
*NNH	0.21	0.04
$*NNH_2$	0.17	0.05
$*NNH_3$	0.23	0.07
*N	0.08	0.04
*NH	0.28	0.06
$*NH_2$	0.67	0.06
$*NH_3$	0.87	0.13

Table S5. The DFT Calculated zero point energies E_{ZPE} and *TS* of different intermediates, where the * denotes the adsorption site on the Fe-MoS_2 catalyst.

Intermediate	E_{ZPE} (eV)	*TS* (eV)
$*N_2$	0.17	0.09
*NNH	0.22	0.04
$*NNH_2$	0.16	0.06
$*NNH_3$	0.24	0.07
*N	0.08	0.04
*NH	0.34	0.05
$*NH_2$	0.69	0.06
$*NH_3$	0.99	0.14

Reference

1. J. Sun, X. Li, W. Guo, M. Zhao, X. Fan, Y. Dong, C. Xu, J. Deng and Y. Fu, *Crystals*, 2017, **7**, 198.
2. X.-H. Zhang, C. Wang, M.-Q. Xue, B.-C. Lin, X. Ye and W.-N. Lei, *Chalcogenide Lett.*, 2016, **13**, 27-34.
3. G. Feng, A. Wei, Y. Zhao and J. Liu, J. Mater. Sci.: Mater. Electron., 2015, 26, 8160-8166.
4. C.-B. Wang and W.-X. Zhang, *Environ. Sci. Technol.*, 1997, **31**, 2154-2156.
5. J. Hafner, *J. Comput. Chem.*, 2008, **29**, 2044-2078.
6. J. P. Perdew, J. A. Chevary, S. H. Vosko, K. A. Jackson, M. R. Pederson, D. J. Singh and C. Fiolhais, *Phys. Rev. B*, 1992, **46**, 6671-6687.
7. P. Atkins, J. de Paulo, Physical Chemistry, 6th edit. WH Freeman, New York, 1998.
8. B. H. R. Suryanto, C. S. M. Kang, D. Wang, C. Xiao, F. Zhou, L. M. Azofra, L. Cavallo, X. Zhang and D. R. MacFarlane, *ACS Energy Lett.*, 2018, **3**, 1219-1224.